Physics – Uspekhi **52** (6) 573 – 601 (2009)

ORAL ISSUE OF THE JOURNAL "USPEKHI FIZICHESKIKH NAUK" PACS numbers: **06.20. – f**, 07.55.Ge, **76.70. – r**

Modern radio-optical methods in quantum magnetometry

E B Aleksandrov, A K Vershovskii

DOI: 10.3367/UFNe.0179.200906f.0605

Contents

Abstract. This paper is an extension of a part of the talk delivered under the more general title "Narrow spectral lines in fundamental metrology: state of the art, prospects, and problems" at the session of the 90th anniversary of *Physics–Uspekhi*. The talk reviewed past developments and the current status of the metrology of length, frequency/time, and magnetic fields. The measurement of these quantities currently relies on the high stability of energies of standard transitions between metastable atomic states. Because of space restrictions in the journal, all metrology topics other than the title one were omitted in the present review.

1. Introduction

The development of quantum magnetometry, a science finding numerous applications in basic research and technology, dates back to the 1940s, when it originated from the work of Bloch [1, 2] and Varian and Packard [3] (based on measurements of the nuclear magnetic moment by Rabi et al. [4, 5]). These authors proposed measuring magnetic fields from the free precession frequency of the proton magnetic moment. Realization of this idea has led to the creation of *proton magnetometers*, the first instruments for measuring magnetic fields in *absolute* terms, i.e., based only on fundamental constants (in this case, the proton gyromagnetic ratio) and variables derived from them, e.g., frequency.

For all the advantages of proton magnetometers, three main drawbacks restrict the scope of their application: cyclic operation precluding continuous field measurement, very low static nuclear susceptibility, and a relatively small proton precession frequency that takes at least a few tenths of a second to be measured precisely.

The works of Overhauser [6, 7] and Slicher and Carver [8] demonstrated the possibility of more than a thousand-fold increase in the degree of proton spin polarization by the dynamic nuclear polarization method. Magnetometers based on this principle are named after Overhauser. Later, they were modified for continuous measurement.

The development of radio-optical quantum methods for the measurement of magnetic fields was given impetus by two events that occurred almost simultaneously in the mid-20th century: the invention of *optical detection* of a magnetic resonance by Bitter [9] and the discovery of *optical pumping* by Kastler [10, 11].

These events stimulated rapid development of quantum magnetometry and gave rise to a family of optically pumped quantum magnetometers (OPQMs). These instruments provided extremely high absolute precision and sensitivity in magnetic field measurement (see, e.g., reviews [12–17]). Apart from their unprecedented accuracy, quantum magnetometers surpass even superconducting quantum interference device (SQUID) magnetometers in terms of variational sensitivity [18]. True, competition between devices of these two classes is purely nominal, the physical principles of their operation and fields of application being quite different. Quantum magnetometers are used to measure magnetic field strength, whereas SQUIDs serve to determine incremental magnetic flux through a superconducting contour; their readings are not absolute (even though work is underway to develop SQUID-based absolute measurement devices [19]).

E B Aleksandrov, A K Vershovskii Ioffe Physical Technical Institute, Russian Academy of Sciences,
ul. Politekhnicheskaya 26, 194021 St. Petersburg, Russian Federation
Tel. (7-812) 297 31 04
E-mail: ealexandrov@bk.ru, antver@mail.ru

Received 24 April 2009
Uspekhi Fizicheskikh Nauk **179** (6) 605 – 637 (2009)
DOI: 10.3367/UFNr.0179.200906f.0605
Translated by Yu V Morozov; edited by A M Semikhatov

In what follows, by quantum magnetometers we mean optically pumped devices, to avoid confusion with proton magnetometers and SQUIDs not considered in this review. Special attention is given to a potassium narrow-line magnetometer [20, 21] with unique characteristics that distinguish it even from other OPQMs.

2. The optical pumping method

2.1 Double radio-optical resonance and optical orientation of atomic and nuclear moments

All radio-optical quantum magnetometers are one way or another based on the use of *optical pumping* and *double radio-optical resonance* methods. The principle of optical pumping consists of selective optical excitation of magnetic and/or hyperfine sublevels in the structure of atomic ground and metastable states that perturbs the Boltzmann distribution of its populations. Optical pumping that modifies the relative population of magnetic (Zeeman) sublevels and leads to the appearance of a nonzero macroscopic dipole magnetic moment in matter is referred to as *optical orientation*. There are optical methods for the creation of a macroscopic quadrupole magnetic moment (alignment) and higher-order moments.

The physical basis of the optical pumping process is described in many publications dating from the 1950s; the review by Happer [27] is worthy of special note as the most informative and comprehensive one, along with a few others [22–26].

The double radio-optical resonance (DRR) method is typically used in combination with optical pumping. In this method, conditions are created under which absorption or emission of a certain amount of radiofrequency quanta by an atomic system alters the number of absorbed and/or re-emitted photons; this change can be detected in experiment. It allows improving the sensitivity of magnetic resonance detection by many orders of magnitude compared with that of ordinary radiospectroscopy because the efficiency of optical quantum recording can reach unity.

One of the DDR methods is stimulated Raman scattering that does not imply direct action of the radiofrequency field on the atom. A typical example is the so-called lambda system, in which two lower sublevels of the atom are coupled to the common excited level by two coherent optical harmonics whose frequency difference corresponds to the distance between the lower sublevels and lies in the radio-frequency region.

The energy of an atom in a magnetic field is given by the scalar product of the magnetic induction and magnetic moment vectors. In the case of a purely electron or purely nuclear moment, the frequency interval between the adjacent levels characterized by quantum numbers m_s and $m_s \pm 1$ (or m_I and $m_I \pm 1$ respectively) linearly depends on the magnetic field induction $B = |\mathbf{B}|$, with the gyromagnetic ratio playing the role of the proportionality coefficient:

$$\omega = \frac{\Delta E}{\hbar} = \gamma B . \tag{1}$$

The frequency ω (the so-called Larmor frequency) has the meaning of a magnetic moment precession frequency; it is measured in the majority of magnetometric schemes. In the general case, the Larmor frequency exhibits a nonlinear dependence on the magnetic field.

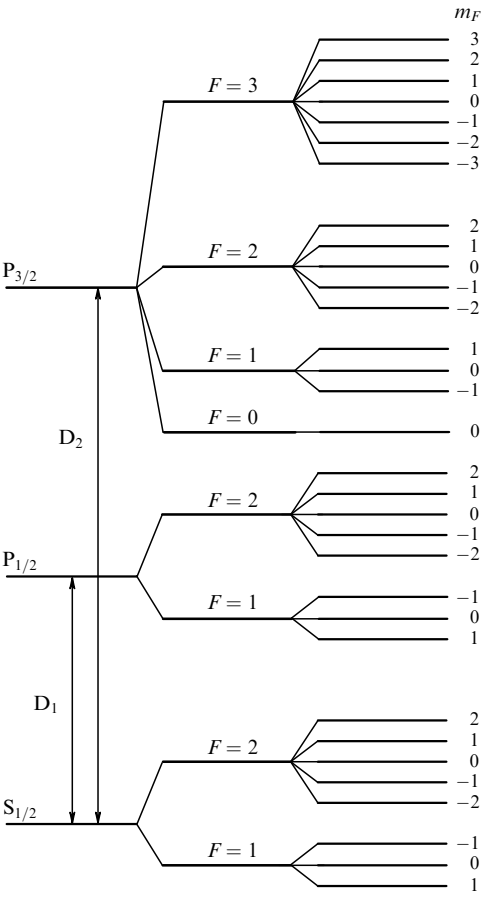

Figure 1. Level diagram (ground and first excited states) of an atom with $I = 3/2$ (isotopes ^{7}Li, ^{23}Na, ^{39}K, ^{41}K, ^{87}Rb). (The splittings are not to scale.)

For an atom having both orbital and spin angular momenta, the total magnetic moment $\boldsymbol{\mu}_J$ of the electron shell, equal to the sum of projections on the **J**-direction of the shell orbital $\mathbf{m}_L$ and spin $\mathbf{m}_s$ magnetic moments, is expressed in Bohr magnetons via the *Lande factor*,

$$g_J = -\left[1 + \frac{J(J+1) + S(S+1) - L(L+1)}{2J(J+1)}\right], \tag{2}$$

with $|\mu_J| = g_J \mu_B \sqrt{J(J+1)}$. There is a similar expression for the g-factor of the total angular momentum of atomic motion $\mathbf{F} = \mathbf{J} + \mathbf{I}$ with a nuclear spin **I** in weak magnetic fields:

$$g_F = g_J \frac{F(F+1) + J(J+1) - I(I+1)}{2F(F+1)} + g'_I \frac{F(F+1) + I(I+1) - J(J+1)}{2F(F+1)} , \tag{3}$$

where g_J and g'_I are the electron and nucleus g-factors, $g'_I = g_I(m/m_p)$.

In strong magnetic fields, the coupling between **I** and **J** is broken down, and the projection of the total atomic momentum is determined by the sum of projections of its components.

The pumping of alkali metals (Fig. 1) and ^{4}He in the metastable state $2\,^3S_1$ is most widely used in quantum magnetometry. The same is true of nuclear paramagnets

(odd isotopes of mercury, ^{199}Hg and ^{201}Hg, in the ground $6\,^1S_0$-state) and helium isotope ^{3}He in the ground state $1\,^1S_0$.

The ground state $n\,^2S_{1/2}$ of alkaline metals characterized by the orbital moment $L = 0$ and spin moment $S = 1/2$ is split into two sublevels, $F = I \pm 1/2$, due to hyperfine interaction. The first excited state of alkali metals is a doublet, $n\,^2P_J$ ($L = 1$, $S = 1/2$, $J = L \pm S = 1/2, 3/2$); each of its lines is in turn split into several hyperfine sublevels in agreement with the allowed values of the quantum number $F = |J - I| \ldots J + I$.

The nuclear spin is $I = 3/2$ for isotopes ^{7}Li, ^{23}Na, ^{39}K, ^{41}K, and ^{87}Rb; $I = 5/2$ for ^{85}Rb; and $I = 7/2$ for ^{133}Cs.

Spectral characteristics of substances used in optical pumping schemes are presented in Refs [22, 25, 27].

Expression (3) adequately describes a linear and equidistant magnetic splitting due to its negligible smallness compared with the hyperfine splitting. However, deviation from the equidistance of magnetic sublevels becomes essential in geomagnetic fields. The exact energy of the alkali metal ground state sublevels is given by the Breit–Rabi equation

$$E\left(I \pm \frac{1}{2}, m_F, \kappa\right) = -\frac{a}{4} - g_I \mu_N B m_F \pm \frac{a}{4}(2I+1)\left[1 + \frac{4m_F}{2I+1}\kappa + \kappa^2\right]^{1/2}, \quad (4)$$

where

$$\kappa = \frac{2\mu_B\left(|g_J| + g'_I\right)}{a(2I+1)} B$$

and a is the hyperfine coupling constant ($\Delta_{HFS} = 2a$ is the hyperfine splitting of the ground state in a zero magnetic field).

Each of the two hyperfine sublevels of the alkali metal ground state in a magnetic field splits into $2F + 1$ sublevels, the transitions with $\Delta m_F = 0, \pm 1$ being permitted in the dipole approximation.

The frequency of transitions $\omega_{m,m-1}$ between sublevels of the same hyperfine state depends on the magnetic field induction vector B. This dependence can be expanded in a power series in B: $\omega_{m,m-1} = a_F B + (1 - 2m) b B^2 \ldots$, the linear terms of the expansion being identical for all the $2F$ transitions making up the Zeeman spectrum of a single hyperfine state. The distance between the components of this spectrum at the frequency scale is largely determined by the quadratic term in b, which is in turn inversely proportional to the hyperfine coupling constant.

Optical detection of Zeeman transitions dates back to the work of Bitter [9] published in 1949, which theoretically demonstrated the possibility of detecting magnetic resonance of excited atomic states from intensity variations of light emitted by the atoms. In the same year, French researchers Kastler and Brossel proposed implementing Bitter's idea of the DDR method [28] as a tool for the radiospectroscopy of short-lived excited atomic states; they later used this method to study the excited mercury state $6\,^3P_1$ [29].

Extension of the DDR method to atomic ground states became possible after Kastler [10] developed the *optical pumping* method in the early 1950s. This method can be briefly described as follows. We consider the ground state comprising two sublevels 1 and 2, and an excited level. If the probability of transitions between the two sublevels is low compared with that of optical excitation, selective excitation of sublevel 1 diminishes its population by increasing the population of sublevel 2. Kastler proposed detecting magnetic resonance from variations in the intensity and polarization of the light emitted by the atoms. Success of the method depends first and foremost on the possibility of maintaining a low relaxation rate between sublevels 1 and 2. Spontaneous relaxation is negligibly slow for radiofrequency and microwave magnetodipole transitions. However, relaxation due to other causes, e.g., interatomic collisions, may be very fast. In his first experiment, Kastler avoided relaxation using an atomic beam in which atom–atom collisions were virtually absent along the entire trajectory. In that experiment, the atomic relaxation time at ground state sublevels estimated from the atom transit time was of the order of 10^{-4} s.

The next step was the use of gas cells. It was found in experiment that the relaxation of angular momentum caused by collisions with the walls of a cell can be prevented by its filling with a buffer gas. The gas slows down diffusion of oriented atoms toward the walls, but collisions with it must not affect orientation. Many gases, most of all inert ones, turned out to meet this condition. The electron state S lacking orbital momentum proved to be extremely stable and preserved the spin state during collisions with atoms and molecules devoid of electron spin.

Similar and even better results than those by filling with a buffer gas can be obtained by coating the inner cell surface with paraffin or polysiloxane, in analogy with the previously developed technology of teflon deposition in the storage chamber of a hydrogen maser. Such coatings are characterized by an abnormally low adsorption energy with respect to alkali metals, such that the time they spend bound to the walls of the cell is too short (some 10^{-10} s) for the electron spin relaxation to occur.

The two methods for slowing down spin relaxation use different pumping mechanisms. In a coated cell, an atom spends most of the time in free flight. Hence, the probability of its perturbation in the excited state is low. In contrast, an excited atom is involved in several collisions when in the buffer gas. Unlike the ground state having only a spin momentum, the excited state of an atom is characterized by the orbital momentum very sensitive to collisions, its reorientation cross section being 10^{-14}–10^{-15} cm^2. Therefore, the angular momentum in the excited state becomes totally randomized at the pressure of several torrs (a higher pressure of tens and hundreds of torrs is typically used); this accounts for an equiprobable population of all sublevels of the ground state during spontaneous emission. The pumping process of this type depends only on light absorption patterns: the levels become depleted at maximum absorption. The difference between the two pumping techniques is especially well apparent when alkaline earth metals are pumped at a single resonance D_2-line. Pumping in a cell with a coated inner surface results in population of the level with the maximum angular momentum projection, i.e., the maximally absorbing level. The same level is greatly depleted during pumping with a buffer gas. In contrast, as was first noted in [30], the D_1-line pumping is qualitatively identical in either case because the level with the maximum momentum projection absorbs no light and undergoes maximum population.

In the first optical pumping experiments, changes in the population under the effect of pumping light were estimated from variations of the scattered light polarization. Later studies demonstrated the higher efficiency of recording the population distribution from the intensity of absorption of

light passing through the cell. This method of registration was first proposed by Dehmelt [31]. Alternatively, polarization of the medium can be detected from polarization rotation of off-resonant light (the paramagnetic Faraday effect [32]).

2.2 Elementary theory of optical pumping

A rigorous theory of optical pumping allowing computation of the values of atomic density matrix elements as functions of time, frequency, and intensity of light and radiofrequency field must be a quantum one. In other words, it must consider atom interactions with a quantized electromagnetic field. Such a theory is rather complicated, although a number of simplified approaches are available (see, e.g., Ref. [25]). One is a simple calculation of the population of ground state sublevels under the action of pumping light that can be reduced to the solution of a set of balance equations. This approach permits assessing the dynamics and stationary values of populations of ground state sublevels in the absence of a radiofrequency field.

Variation of populations of ground state sublevels in time under the effect of optical pumping and relaxation can be described by the system of differential balance equations [30]

$$\frac{\mathrm{d}p_k}{\mathrm{d}t} = -\sum_{j=1}^{n}(b_{kj}+w_{kj})\,p_k + \sum_{i=1}^{n}(b_{ik}+w_{ik})\,p_i\,, \qquad k = 1,2,\ldots,n\,, \tag{5}$$

where the p_j are populations of ground state sublevels, b_{ij} is the probability of atomic transitions (per unit time) from state i to state j as a result of photon absorption and reemission, and w_{ij} is the corresponding probability of a nonoptical (relaxation) transition. The number of independent equations is $n-1$ by virtue of the additional normalization equation $\sum_k p_k = 1$ corresponding to the weak pumping case.

The probability that an atom in state k absorbs a photon is given by $\sum_j b_{kj}$. The probability β that any atom absorbs a photon then follows by summation over all n sublevels of the ground state, $\beta = \sum_k \sum_j b_{jk}\,p_k$. Assuming an equal probability $(1/n)$ of a population of each of the n sublevels under thermal equilibrium, we obtain the average probability of photon absorption by an atom prior to orientation as

$$\beta_0 = \int_0^\infty I_\nu \sigma_\nu \,\mathrm{d}\nu = \frac{1}{n}\sum_k \sum_j b_{jk}\,. \tag{6}$$

Here, I_ν is the spectral density of exciting light and σ_ν is the optical absorption cross section at an equal population of the ground state sublevels.

The assumption that all probabilities of thermal relaxation transitions $w_{jk} = w$ are identical (as they actually are) simplifies the equations. Moreover, all the coefficients b_{ij} vanish if pumping is switched off at a certain moment, and Eqn (5) acquires the form

$$\frac{\mathrm{d}p_k}{\mathrm{d}t} = -\frac{p_k - 1/n}{T}\,, \tag{7}$$

where $T = 1/w$.

Equation (7) corresponds to an exponential relaxation of the population of each level toward an equilibrium value with a time constant T.

A stationary analytic solution of (5) can easily be found in the case of complete mixing in the exited state. In this case, b_{ik} is independent of the final sublevel k, i.e., $b_{ik} = b_i$. Equating the rate of level population changes to zero and assuming the independence of thermal relaxation from the level number leads to

$$p_k = \frac{1}{(w+b_k)\sum_j 1/(w+b_j)}\,. \tag{8}$$

Expression (8) means that the population of any sublevel in the case of complete relaxation of angular momentum in the excited state is determined by the probability of an atom escaping from this sublevel under the action of light and relaxation processes. This type of optical pumping is sometimes referred to as 'depumping' to distinguish it from 'repumping,' under which the excited atom preserves its angular momentum [27].

System of equations (5) can be solved numerically even in the absence of the angular momentum relaxation; such a solution is proposed in Ref. [30] for atoms with $J = 1/2$, $I = 3/2$ (^{23}Na, ^{39}K, ^{41}K, ^{87}Rb), in the case of excitation by circularly polarized light of the D_1-line; relative populations of levels in the stationary case are given depending on the factor $\rho = 1/\beta_0 T$ that determines the efficiency of optical pumping. It was shown, in particular, that the D_2-line pumping (unlike the D_1-line momentum relaxation) changes sign upon introduction of pumping in the excited state. Generally speaking, the presence of the D_2-line in the case of D_1-pumping impairs the orientation of matter. Therefore, the D_1-line pumping is needed if a high degree of orientation is to be achieved. The results of the solution of an analogous system for D_1- and D_2-lines are also presented in [25, p. 112].

2.3 Level shifts in optical pumping

When inducing transitions from the ground to an excited state, the pumping light causes not only broadening of resonant transitions in the ground state structure but also shifts of two major types. One is given by shifts induced by the optical Stark effect proportional to the pumping intensity. The Stark shift is deduced from the perturbation theory. The correction ΔE_j for the jth energy level is given by [33]

$$\Delta E_j = \sum_k \frac{|V_{jk}|^2}{E_j - E_k \pm \hbar\omega}\,, \tag{9}$$

where V_{jk} is the matrix element of transition between the initial level j and any intermediate level k with the energy E_k under the action of light with the frequency ω. The negative sign is chosen if the energy of level k is higher than that of j, and the positive sign is chosen otherwise. The above equation implies that the frequency of the applied field differs from the resonant frequency by a quantity exceeding the transition width; otherwise, the width of the level must be taken into account to avoid divergence. The sum extends over all possible atomic states; however, only terms close to the resonance ones may be considered for practical purposes. At resonance, levels are not shifted, but each splits if the field is strong enough and the matrix element V_{jk} exceeds the level width.

It is assumed in Eqn (9) that the perturbation field is monochromatic and the transition frequency is fixed. In passing to real objects, such as Doppler-broadened absorption lines, the shift should be averaged over the atomic frequency distribution.

The result is the dependence of the shift on the frequency detuning proportional to the function $S(\nu - \nu_0)$, i.e., the

convolution of the dispersion and Doppler contours (the Voigt integral)

$$S(\nu-\nu_0)=\Phi(\nu')=\int_{-\infty}^{\infty}\frac{x-\nu'}{(x-\nu')^2+\alpha^2}\exp(-x^2)\,\mathrm{d}x, \quad (10)$$

where ν is the field harmonic frequency for which the shift is sought, reduced to the Doppler width, ν_0 is the frequency at the absorption line center reduced to the Doppler width, and α is the ratio between the uniform transition width and the Doppler width.

Formula (10) takes only one transition at the frequency ν_0 into account. The total shift can be found by summing over all excited states within a given optical line, i.e., over all hyperfine sublevels taking account of their transition strength. If the excitation is induced by a finite-width spectral line (in contrast to a single-mode laser excitation), then the result must be additionally averaged over the line profile.

The operator formalism of the description of the interaction between atoms and pumping light was developed by Happer and co-workers in Refs [34–36]. These authors derived formulas describing the absorption of pumping light and the resulting level shifts in an atomic system.

There is one more mechanism of resonant frequency shifts related to *real* transitions. Its role becomes noticeable when an excited atom avoids collisions and preserves its polarization after transition to the ground state. Due to the difference between g-factors of the excited and ground states, its phase becomes shifted with respect to the phases of atoms continuing to precess in the ground state. The mechanism of this shift is known as *coherence transfer*. Expressions for the shift caused by real transitions are given in Ref. [36]. These shifts are always negative for alkali metals because the gyromagnetic ratio for the excited state is smaller than for the ground state or even has the opposite sign. The shifts are proportional to the magnetic field strength (until the additional phase increment for the lifetime of the excited state exceeds 1 radian). Importantly, such shifts never exceed the line broadening under the effect of pumping light, whereas the Stark shift may be much greater than the light-induced broadening.

2.4 Methods of optical pumping

The variety of optical pumping methods can be arbitrarily categorized into *direct* and *indirect* [22, 27]. The former comprise processes in which the nonequilibrium state of matter results from direct interaction of atoms (molecules) with light. In the latter group, the direct optical pumping of atoms of an intermediate element is followed by a transfer of the acquired orientation to the main object through interatomic collisions.

Indirect optical pumping is necessary because direct methods are suitable only for a limited number of atoms and require a combination of specific conditions to be applied, the main ones being that the object must have absorption lines in the accessible spectral region and fine splitting must be optically resolvable.

2.4.1 Polarization pumping. Polarization pumping by circularly polarized light is referred to as *optical orientation* and the atomic ensemble is said to be *oriented*. Also possible is polarization pumping by linearly polarized and even unpolarized light. This process is known as *optical alignment* and the atomic ensemble is then called '*aligned*.' Such a state is characterized by different populations of sublevels having different absolute values of angular momentum projections (i.e., sublevels with different $|m_F|$), whereas sublevels differing only in the projection sign are similarly populated. In the spherical representation, atoms in this state have a nonzero quadrupole magnetic moment.

Expansion of the atomic magnetic moment in spherical harmonics was proposed in [37] and further developed in [38] and [27]. In accordance with this concept, the entirely spherical distribution of the moment corresponds to the identical population of all Zeeman sublevels or to the zero moment. The purely dipole moment is characterized by an asymmetric distribution of sublevel populations increasing from the sublevel with the smallest m_F to that with the largest m_F (or, vice versa, depending on the moment's sign). Even moments are characterized by a symmetric distribution of populations of the Zeeman sublevels. The state in which all atoms are concentrated in a single magnetic sublevel (when $F>1/2$) is a mixed state characterized by the presence of all the harmonics possible in a given configuration.

The spherical representation of the atomic moment has certain advantages regarding the description of optical pumping processes. First, neither constant nor oscillating magnetic fields can affect the distribution of spherical harmonics of the magnetic moment. Second, it can be shown that for isotropic relaxation, each spherical harmonic of the magnetic moment relaxes at its own rate independent of other harmonics. Third, only dipole and quadrupole atomic moments participate in all linear processes of light absorption and emission. Therefore, octupole and higher moments can be excluded from the consideration of optical pumping if the processes are actually linear.

2.4.2 Spectrum-selective pumping. In *spectrum-selective* optical pumping, the only meaningful difference between sublevels of the ground state is their energy. If the excitation spectrum is formed such that atoms are excited only from a certain energy sublevel, this sublevel becomes depleted ('burns down'). This pumping technique is feasible when the ground state structure of interest is greater than the Doppler width of the absorption line. The most efficacious pumping source is a tunable laser with the spectral linewidth smaller than the Doppler width. Traditionally, gas-discharge lamp excitation is used for practical purposes, and the desired excitation spectrum is obtained either by isotopic filtration methods, i.e., by pumping one compound with the resonance emission of another (as a rule, different isotopes of the same elements are used) or with its own resonance radiation filtered through vapors of a different compound. The most common example is given by two stable rubidium isotopes, ^{87}Rb and ^{85}Rb, with partly overlapping Doppler contours of resonance lines. Spectrum-selective pumping finds application in the Rb frequency reference and in magnetometers using microwave transitions in the hyperfine structure of ^{39}K and ^{87}Rb vapors (so-called HFS magnetometers). In both cases, the light from a gas-discharge lamp filled with the vapors of a relevant isotope passes through a cell containing vapor that selectively absorbs the longwave component of the hyperfine structure of resonance lines. A molecular gas, e.g., nitrogen, is added to the filter to suppress its luminescence containing the longwave line. The shortwave component remaining after filtration selectively pumps vapors in the work cell and thereby predominantly populates the upper hyperfine state $F=2$.

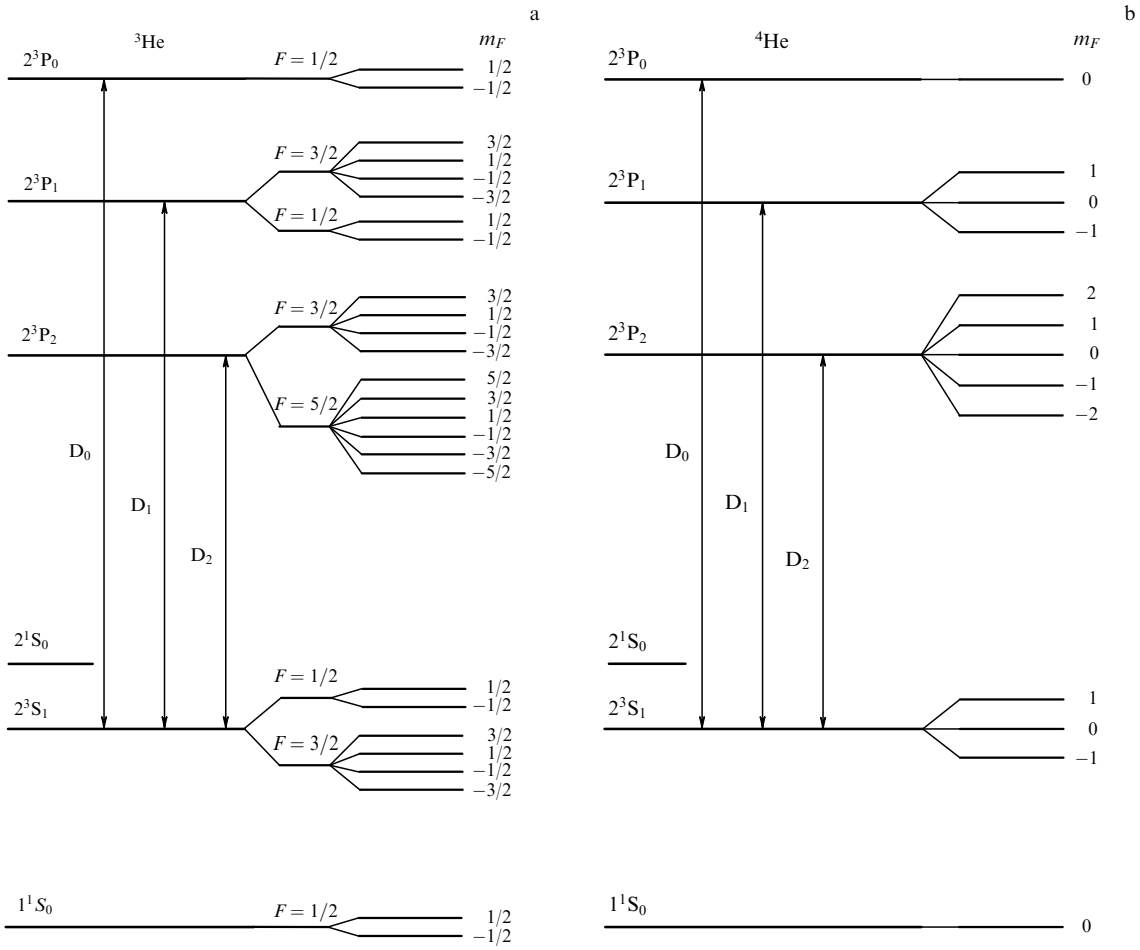

Figure 2. Level diagram of helium isotopes ^{3}He, ^{4}He. (The splittings are not to scale.)

2.4.3 Spin-exchange method. The *spin-exchange* method consists in preparation of a gas mixture containing particles to be oriented and atoms undergoing direct optical orientation. Collisions create a probability of spin orientation transfer from the donor to the acceptor, which does not contradict the conservation laws for the angular momentum and its projection. Collisions give rise to short-lived molecules with shared external electrons. There is a high probability of spin exchange after disintegration of these molecules. The process of exchange for electron spins has a cross section of the order of 10^{-14} cm^2.

Free electrons [39] and hydrogen atoms were the first to be oriented by this method. Orientation of the acceptor in such experiments is deduced from that of the donor using that forced disorientation of the acceptor coincides with impaired donor orientation detected from pumping light absorption. Certainly, such a many-step procedure is less efficacious than direct orientation, but resonance signal intensity decreases only severalfold.

Spin exchange can transfer the electron spin orientation to the nucleus. The first attempt to orient ^{3}He nuclei by exchange with optically oriented rubidium was undertaken in [40]. Later studies, e.g., Ref. [41], demonstrated that the cross section strongly depends on the atomic number of a paramagnet (such orientation is very fast for xenon nuclei). It was shown that the transfer of angular momentum occurs as a molecule is formed in which an alien electron is involved in hyperfine interaction with the paramagnetic nucleus. In a purely transit-time interaction, collision lasts some 10^{-12} s or is much shorter than the hyperfine frequency period. However, if a triple collision gives rise to a molecule that survives until the next collision, the interaction time may greatly increase to be of the order of the inverse hyperfine splitting (usually hundreds or thousands of megahertz); this leads to efficacious magnetization of the nucleus.

2.4.4 Exchange of metastability. Orientation through *metastability exchange* has been described for a single object (^{3}He isotope). In accordance with the Pauli principle, both electrons of the helium atom remain in the low-energy state ($l = 0$, $n = 1$) only when they have opposite spin moments, such that the total spin of the atom is $S = 0$ (state 1^1S_0 — *parahelium, singlet series*). The ^{4}He nucleus having no magnetic moment of its own, the atom of helium-4 is diamagnetic in this state (Fig. 2b).

In another state of the helium atom (*orthohelium, triplet series*), spin moments are unidirectional, building up a resulting spin $S = 1$; in other words, one atom of helium-4 in this state has a nonzero intrinsic moment, i.e., it is paramagnetic. In accordance with the Pauli principle, one electron must be in a state differing from the state of the other in n and l. Of all such states, the state with $n = 2$, $l = 0$ (state 2^3S_1) has the lowest energy.

Transitions between para- and orthostates are forbidden. Therefore, the lifetime of the lowest level may be as long as a few milliseconds, i.e., the level is metastable. The nearest

excited level of orthohelium is the 2P level ($L = 1$) split into three sublevels as a result of the spin–orbital interaction.

The difference between ^{3}He and ^{4}He spectra is due to the nuclear spin $I = 1/2$ in ^{3}He. The ground 1^1S_0 parastate of ^{3}He has the property of nuclear paramagnetism and splits into two Zeeman sublevels, whereas the ground 2^3S_1 orthostate has a hyperfine structure (Fig. 2a).

The metastable state 2^3S_1 has spin 1 and can be oriented. Exposure of the helium gas to a gas discharge under the pressure of several torrs leads to the accumulation of atoms in metastable states having lifetimes of several milliseconds and largely depends on wall relaxation. The lifetime of the metastable state cannot be prolonged by wall coating because metastable helium atoms have an excess energy (approximately 19 eV) sufficient to ionize any other atom but helium. For an atom in the metastable state, only collisions with helium atoms in the ground state playing the role of a buffer gas are nondestructive.

Metastable atoms are subject to optical pumping by resonance triplet lines $2^3S_1 \Rightarrow 2^3P_{0,1,2}$ with wavelengths in the vicinity of 1.083 μm. Collision between an oriented metastable helium atom and an atom in the ground state may result in the exchange of metastability [42]. In the case of ^{4}He, the angular momentum of the ground state and its projection are conserved. Therefore, the exchange has no effect on the overall orientation of the ensemble of metastable atoms.

The situation is different in experiments with ^{3}He isotopes that have a nuclear moment. Collision between helium atoms in metastable and ground states may result in an exchange of nuclear spin directions. In other words, a new relaxation channel of the metastable state moment emerges that immediately manifests itself as well-apparent broadening of magnetic resonance lines in the 2^3S_1 state. The linewidth for ^{4}He is of the order of 1 kHz, whereas the linewidth for ^{3}He is several hundred times greater.

Metastability exchange allows efficacious ($> 50\%$) polarization of the ^{3}He ground state [42, 43].

2.4.5 Spin-selective ionization. One more specific orientation mechanism relies on the angular momentum transfer in atom–atom collisions. We consider optically oriented helium in a metastable state. The presence of an impurity atomic gas with angular momentum in the ground state leads to collisions resulting in the ionization of impurity atoms and transition of helium atoms to the ground state. The physical basis of this process discovered by Penning et al. in 1937 [44] (*Penning ionization*) is considered at greater length in [44].

We emphasize that ionization obeys the spin momentum conservation law. If an impurity atom has a single electron, ionization produces a free electron, an ion, and an atom of helium in the ground state; only the electron has an angular momentum. That sum of momenta prior to the reaction are equal to the electron angular momentum places a limitation on the character of the reaction, which proves to be spin-dependent; that is, certain mutual orientations of helium and impurity atoms disappear in the course of ionization and the initially disoriented ensemble acquires orientation. In this way, orientation is transferred from optically oriented alkali metals to metastable helium atoms [45–47] and from helium atoms to ionized two-electron atoms. Polarization experiments with atomic ions of the second group (Zn, Sr, and Cd) colliding with optically oriented helium atoms are described in Ref. [48].

3. Evolution of the magnetic moment in an external magnetic field

3.1 Classical consideration

Bloch [1] was the first to derive phenomenological equations of magnetic resonance in terms of the motion of Cartesian components of the magnetic moment vector under the effect of constant and alternating magnetic fields, taking relaxation processes into account. Later, Feynman [49] showed that these equations are in excellent agreement with quantum consideration of the problem of spin $S = 1/2$ motion in a magnetic field. Moreover, they are applicable to the problem of motion of averaged Cartesian components of an arbitrary magnetic moment. Thereafter, it became clear that the problem of the behavior of an arbitrary two-level system interacting with a harmonic field is also reducible to Bloch equations [50]. Most quantum systems are characterized by a nonequidistant localization of energy levels. Therefore, a typical problem of spectroscopy, i.e., elucidation of the system response to a monochromatic field with adjustable frequency, reduces to a large number of independent problems of the interaction between two-level systems and a monochromatic field because interaction outside the resonance area can be disregarded. A criterion for the permissiveness of neglect is the ratio of the matrix element V_{jk} of the coupling to the field to level widths and the remoteness of the field frequency from the resonance.

The equation for the rotational motion of a point mass about an axis under the action of a force $\mathbf{F}$ at an arm $\mathbf{R}$ is derived from the Newton equation $\mathrm{d}\mathbf{p}/\mathrm{d}t = \mathbf{F}$ by vector multiplication by $\mathbf{R}$:

$$\frac{\mathrm{d}\mathbf{M_p}}{\mathrm{d}t} = \mathbf{M_F}\,. \tag{11}$$

Here, $\mathbf{M_F} = \mathbf{F} \times \mathbf{R}$ is the moment of force and $\mathbf{M_p} = \mathbf{p} \times \mathbf{R}$ is the angular momentum.

If a system has not only mechanical angular momentum but also a magnetic moment $\mathbf{M}$ proportional to it with a coefficient γ, $\mathbf{M} = \gamma\,\mathbf{M_p}$, then the action of a magnetic field $\mathbf{B}$ creates the moment of force equal to $\mathbf{M} \times \mathbf{B}$. Rewriting Eqn (11) for the magnetic moment $\mathbf{M}$ gives the simplest Bloch equation describing the motion of $\mathbf{M}$ in an arbitrary (e.g., alternating) magnetic field $\mathbf{B}$:

$$\frac{\mathrm{d}\mathbf{M}}{\mathrm{d}t} = \gamma\,\mathbf{M} \times \mathbf{B}\,. \tag{12}$$

In the specific case of a constant field B_0 directed along the z axis, i.e., $B_z = B_0$, $B_x = B_y = 0$, the moment component along the z axis remains constant, whereas its transverse component rotates about z with the frequency $\omega_0 = \gamma B_0$.

We introduce a reference frame x', y', z rotating about the z axis with an angular speed ω. Application of the vector transformation rule to Eqn (12) yields

$$\frac{\mathrm{d}\mathbf{M}}{\mathrm{d}t} = \gamma\left[\mathbf{M} \times \left(\mathbf{B} - \frac{\omega}{\gamma}\right)\right] = \gamma\,\mathbf{M} \times \mathbf{B}' \tag{13}$$

in the rotating system. Thus, the magnetic field vector in the rotating system of coordinates experiences the action of an effective magnetic field $\mathbf{B}'$ diminished by ω/γ compared with the initial field $\mathbf{B}$. This result is known as Larmor's theorem.

Passing to the rotating reference frame, it is easy to solve the problem of magnetic resonance, i.e., of the magnetic moment evolution in a constant magnetic field under the

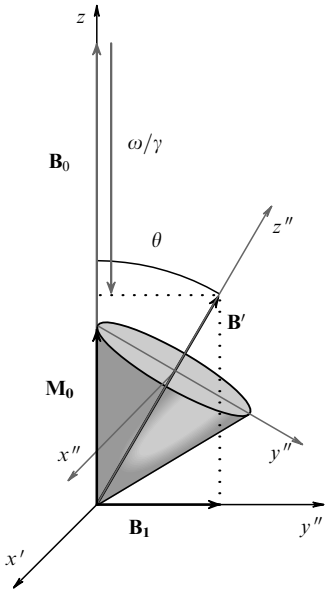

Figure 3. Evolution of the magnetic moment in an alternating magnetic field.

action of an alternating magnetic field $\mathbf{B}_1$ rotating about the z axis with a frequency ω (Fig. 3). Let the magnetic moment M_0 be directed along the z axis at $t = 0$. We pass to the system of coordinates rotating with the angular speed ω. In this system, the moment undergoes the action of a constant field $\mathbf{B}'$ equal to the vector sum of the field $B_0 - \omega/\gamma$ along the axis and the field $\mathbf{B}_1$ directed perpendicular to the z axis (along the y' axis of the rotating coordinate system). The vector $\mathbf{M}$ precesses around the direction of $\mathbf{B}'$ without changing its length with the frequency

$$\omega' = (\Delta\omega^2 + \Omega^2)^{1/2}\,, \tag{14}$$

where $\Delta\omega = \omega_0 - \omega$ is the detuning of the alternating field frequency, $\omega_0 = \gamma B_0$ is the magnetic resonance frequency, and $\Omega = \gamma B_1$ is Rabi's frequency of the alternating field.

Calculation of the moment vector projections on the laboratory reference frame axes is reduced to a purely geometric problem solvable by passing to a new system of coordinates in which the vector $\mathbf{B}'$ is directed along the z'' axis and by the reverse transition to the laboratory reference frame.

It turns out that in the laboratory system of coordinates in the vicinity of a resonance, the magnetic moment vector moves along the spiral curve over the surface of a sphere. The locus of points making up the totality of solutions of Bloch equation (12) and known as the *Bloch sphere* is frequently used in quantum mechanics for the description of the state of two-level system (20). The upper and lower poles of the sphere are respectively regarded as its north and south poles, and the plane $z = 0$ is called the equator. We use this nomenclature in what follows.

Thus, the projection of the moment on the equatorial plane in the laboratory system of coordinates rotates with a circular frequency equal to the frequency of the applied alternating field. Movements over the sphere from north to south pole and back are harmonic with the nutation frequency $\omega' = (\Delta\omega^2 + \Omega^2)^{1/2}$. Infinitely far from the resonance, the nutation frequency tends toward the alternating field frequency ω and the nutation amplitude vanishes. As the field frequency approaches the resonance, the nutation frequency decreases to the Rabi frequency $\Omega = \gamma B_1$. At the same time, the nutation amplitude increases and a hodograph of the magnetic moment vector in resonance extends over the entire sphere, from north to south pole.

Taking relaxation processes into account leads to a stationary but not equilibrium state in which the longitudinal magnetization decreases compared with its level in the equilibrium system; simultaneously, periodic motion of the magnetization transverse components emerges at the frequency of the resonance-inducing field, while the nutation is damped out.

In the general case, longitudinal and transverse components of the angular momentum vector may relax differently. It is clear from symmetry considerations that the relaxation times of two transverse components are identical but may be different from the longitudinal relaxation time. Under the assumption of an exponential character of the relaxation, the Bloch equations are written as

$$\begin{aligned}
\frac{\mathrm{d}M_x}{\mathrm{d}t} &= \gamma(M_y B_0 - M_z B_y) - \frac{M_x}{T_2}\,,\\
\frac{\mathrm{d}M_y}{\mathrm{d}t} &= \gamma(M_z B_x - M_x B_0) - \frac{M_y}{T_2}\,,\\
\frac{\mathrm{d}M_z}{\mathrm{d}t} &= \gamma(M_x B_y - M_y B_x) - \frac{M_z - M_0}{T_1}\,.
\end{aligned} \tag{15}$$

This form implies that relaxation processes in the absence of transverse fields with a time constant T_1 bring the longitudinal moment to M_0 (given by the pumping conditions), while transverse components tend to zero with a time constant T_2 ($T_1 \geqslant T_2$).

Passing to the rotating system of coordinates (x', y', z), we use the notation accepted in the literature ($v \equiv M_{x'}$, $u \equiv M_{y'}$), where the rotating component of the moment u is parallel to the alternating magnetic field B_1 and v is normal to it.

In the rotating coordinate system, the magnetic field is time independent, which gives the system of differential equations with constant coefficients:

$$\begin{aligned}
\frac{\mathrm{d}v}{\mathrm{d}t} &= u\Delta\omega - M_z\Omega - \frac{v}{T_2}\,,\\
\frac{\mathrm{d}u}{\mathrm{d}t} &= -v\Delta\omega - \frac{u}{T_2}\,,\\
\frac{\mathrm{d}M_z}{\mathrm{d}t} &= \gamma v B_1 - \frac{M_z - M_0}{T_1}\,.
\end{aligned} \tag{16}$$

The stationary solution is found by equating the left-hand sides of the equations to zero; hence follows an algebraic system of three linear equations with the solutions

$$\begin{aligned}
\mathbf{v} &= -\mathbf{M}_0\,\frac{\Omega T_2}{1 + (\Delta\omega T_2)^2 + \Omega^2 T_1 T_2}\,,\\
\mathbf{u} &= \mathbf{M}_0\,\frac{\Delta\omega\Omega T_2^2}{1 + (\Delta\omega T_2)^2 + \Omega^2 T_1 T_2}\,,\\
\mathbf{M}_z &= \mathbf{M}_0\,\frac{1 + (\Delta\omega T_2)^2}{1 + (\Delta\omega T_2)^2 + \Omega^2 T_1 T_2}\,.
\end{aligned} \tag{17}$$

An exact resonance has no component u; this means that the transverse component of the angular momentum precesses with a 90° shift relative to the B_1 field vector. The steady-state

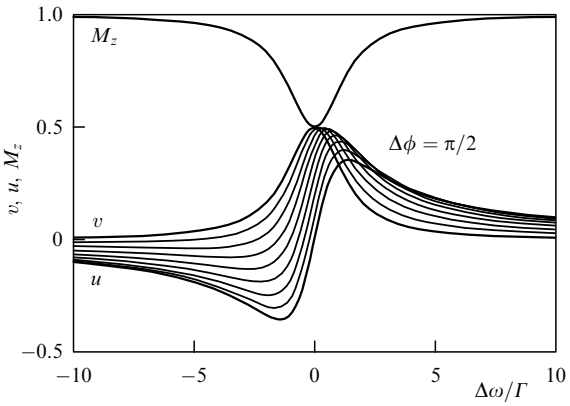

Figure 4. Longitudinal (M_z) and transverse components of the magnetic moment depending on the frequency and phase detuning.

value of longitudinal magnetization, unlike that in transition processes, varies from the initial maximum to zero, depending on resonance conditions, and never changes sign. Absorption of the alternating field energy by the system per unit volume is given by the v component:

$$P = \frac{1}{T}\int_0^T \mathbf{B}\,\frac{\mathrm{d}\mathbf{M}}{\mathrm{d}t}\,\mathrm{d}t = \frac{\pi\omega}{2}\,B_1 v\,. \tag{18}$$

The u component determines dispersion.

In the magnetic resonance technique, a linearly polarized driving field, rather than a rotating field, is typically used. Taking account of the second component of the alternating magnetic field rotating in the opposite direction leads to an additional shift in the resonant frequency (the so-called Bloch–Siegert shift). This shift is approximately equal to $\Omega^2/4\omega_0$; it is neglected in the case of $|B_1| \ll |B|$ as in OPQM systems.

3.2 Types of magnetic resonance signals

Three types of magnetic resonance signals are distinguished according to three projections of the magnetic moment, M_z, u, and v. The first one is associated with a constant magnetization M_z or a related quantity. The magnetization increment ΔM_z caused by the effect of the alternating magnetic field B_1 is usually recorded instead of the magnetization itself.

At low intensity of the field B_1 given by the condition $\Omega^2 T_1 T_2 \ll 1$, the dependence $\Delta M_z(\Delta\omega)$ has a characteristic, so-called Lorentzian form

$$\Delta M_z(\Delta\omega) = M_0\Omega^2 T_1 T_2 L(\Delta\omega T_2)\,, \tag{19}$$

where $L(x) = 1/(1+x^2)$ is the Lorentz contour (Fig. 4).

It is typical in the NMR technique to detect signals produced by forced motion of transverse magnetization. This magnetization induces alternating voltage in any contour enclosing the sample, e.g., in coils used for the alternating field induction. This additional voltage on the inductor can be separated and analyzed, as was first done by the Bloch cross-coil method.

Determination of the signal phase and amplitude by the synchronous detection method allows selectively extracting the components u and v. A signal proportional to the field B_1 is used as a reference, with its phase chosen so as to enable selection of the desired component. For example, a signal proportional to u can be distinguished, with its dispersion-like contour being a function of the detuning $\Delta\omega$. Such a signal shape is most convenient for using resonance as a frequency discriminator: there is no signal at the exact resonance, whereas in the case of detuning, information about its sign is carried in the signal sign. However, close control of the signal phase is needed (phase-dependent changes in shape and, accordingly, the point where it crosses zero are shown in Fig. 4). Phase control becomes unnecessary when the induction signal amplitude or the absorbed power is used as the resonance signal. In this case, however, the signal has the form of an even function with an extremum at the resonance point. This requires low-frequency modulation of detuning and standard synchronous detection of the low-frequency signal for determining the sign and the value of constant detuning.

3.3 Quantum-mechanical (semiclassical) consideration of the problem of interaction between a two-level system and an external field

In 1958, a group of researchers led by Feynman [49] showed that the interaction of any two-level system with an external alternating field yields the same solutions as the problem of magnetic resonance; in other words, the Schrödinger equation for a two-level system,

$$\mathrm{i}\hbar\left(\psi_1\,\frac{\mathrm{d}C_1}{\mathrm{d}t} + \psi_2\,\frac{\mathrm{d}C_2}{\mathrm{d}t}\right) = C_1\mathbf{H}\psi_1 + C_2\mathbf{H}\psi_2\,, \tag{20}$$

can be reduced to Bloch equations. Equivalent to the Schrödinger equation is the Liouville equation for the density matrix

$$\mathrm{i}\hbar\,\frac{\mathrm{d}\boldsymbol{\rho}}{\mathrm{d}t} = [\mathbf{H}, \boldsymbol{\rho}]\,. \tag{21}$$

For a two-level system with an unperturbed Hamiltonian $\mathbf{H}_0$ and a harmonic perturbation $\mathbf{V}(t)$, Eqn (21) can be written, using the normalization condition $\rho_{11} + \rho_{22} = 1$, in the form

$$\begin{aligned} \frac{\mathrm{d}\delta}{\mathrm{d}t} &= \frac{4}{\hbar}\,\mathrm{Im}\,(V_{21}\rho_{12})\,,\\ \frac{\mathrm{d}\rho_{12}}{\mathrm{d}t} &= \mathrm{i}\rho_{12}\omega_0 - \frac{V_{12}\delta}{\hbar}\,, \end{aligned} \tag{22}$$

where $\delta = \rho_{22} - \rho_{11}$, $\omega_0 = (E_2 - E_1)/\hbar$, and E_1 and E_2 are eigenvalues of $\mathbf{H}_0$.

The three equations in (22) (ρ_{12} being a complex quantity) reduce to Bloch equations in the absence of relaxation. Relaxation for populations (T_1) and nondiagonal matrix element (T_2) is introduced as follows:

$$\begin{aligned} \frac{\mathrm{d}\delta}{\mathrm{d}t} &= \frac{4}{\hbar}\,\mathrm{Im}\,(V_{21}\rho_{12}) - \frac{\delta - \delta_0}{T_1}\,,\\ \frac{\mathrm{d}\rho_{12}}{\mathrm{d}t} &= \mathrm{i}\rho_{12}\omega_0 - \frac{V_{12}\delta}{\hbar} - \frac{\rho_{12}}{T_2}\,. \end{aligned} \tag{23}$$

In the rotating field approximation, the perturbation $\mathbf{V}(t)$ has the form $\mathbf{V}\exp(\mathrm{i}\omega t)$. The stationary solution is sought as a constant population difference and the nondiagonal element in the form $\rho_{12}(t) = \rho_{12}\exp(\mathrm{i}\omega t)$:

$$\begin{aligned} 0 &= \frac{4}{\hbar}\,\mathrm{Im}\,(V_{21}\rho_{12}) - \frac{\delta - \delta_0}{T_1}\,,\\ \mathrm{i}\omega\rho_{12} &= \mathrm{i}\rho_{12}\omega_0 - \frac{V_{12}\delta}{\hbar} - \frac{\rho_{12}}{T_2}\,. \end{aligned} \tag{24}$$

By separately writing expressions for real (x) and imaginary (y) parts of ρ_{12},

$$\rho_{12} = x + \mathrm{i}y\,, \tag{25}$$

we obtain three equations analogous to the three Bloch equations for three components of the moment:

$$\begin{aligned} \delta &= \delta_0 + 4yVT_1\,, \\ y &= T_2 x\Delta\omega - \delta T_2 V\,, \\ x &= -T_2 y\Delta\omega\,, \end{aligned} \tag{26}$$

where $\Delta\omega = \omega_0 - \omega$ and $V = V_{12}/\hbar$.

The solution of the last system for the population difference has the form

$$\delta = \delta_0 \frac{1 + (\Delta\omega T_2)^2}{1 + (\Delta\omega T_2)^2 + 4V^2 T_1 T_2}\,. \tag{27}$$

This result coincides with the solution for longitudinal magnetization if $2V$ is regarded as Ω. It can be shown that both real and imaginary parts of the nondiagonal density matrix element are proportional to two transverse magnetization components in the theory of magnetic resonance.

This theory comprehensively characterizes spin; for spins $1/2$, it is suitable to describe three components of the system magnetization, although their description is incomplete because the quantum momentum J in a magnetic field is characterized by $2J+1$ energy levels and, accordingly, by $(2J+1)^2$ density matrix elements. A complete description of such a many-level system is given by quantum Liouville equation (21). An example of a quantum mechanical equation for an eight-level system with optical pumping is given in Ref. [51].

Multiquantum transitions possible in many-level systems can also be used in magnetometric devices. The probability of such processes is much lower than that of transitions with the emission of a single field quantum. They were predicted theoretically in 1929 [52, 53] and observed experimentally in the radiofrequency range, where necessary spectral densities of electromagnetic radiation power are much easier to obtain [54].

Multiquantum transitions in the radiofrequency region between different levels of the magnetic structure of alkali metal atoms were discovered almost simultaneously in experiments by Hughes and Grabner [55, 56] and Kusch [57, 58] with atomic beams, and in the studies of Kastler and Bossel [59] on the optical pumping of sodium atoms.

In recent years, multiquantum resonances have found increasingly wider application in quantum magnetometry, mainly (1) higher-order $n-1$ multiquantum transitions connecting a system of n quasi-equidistant Zeeman levels of the same hyperfine state, and (2) the so-called Λ-scheme, in which two lower levels, 1 and 2, are linked to the common excited level 3 by two coherent waves whose frequency difference corresponds to the distance between the lower levels. Under the resonance conditions, levels 1 and 2 are coupled by a two-quantum transition and become coherent without population of intermediate level 3. This phenomenon is referred to as the *coherent population trapping effect* [60].

This resonance was first described in 1961 by Bell and Bloom [61], who interpreted it in terms of Bloch equations. A similar resonance in the excited state of cadmium atoms reported by Aleksandrov in 1963 [62] was treated in terms of state interference.

Interest in the Λ-scheme has experienced an upsurge after the advent of readily available stable tunable laser sources because coherent population trapping resonance excited and detected in the optical range is characterized by linewidths typical of radio-optical resonance, with the total suppression of broadenings and shifts observed in the visible region.

One more class of phenomena should be mentioned as potentially interesting for quantum magnetometry. These are transition processes and nonstationary responses arising from a change in conditions in which a magnetic resonance is induced on time scales smaller than relaxation times. They are exemplified by nutations manifest as an oscillation of the longitudinal magnetization and a modulation of the transverse magnetization amplitude. At resonance, this amplitude is initially as large as that of the longitudinal magnetization M_0. As a result, this situation is distinct from the steady-state situation, in which the transverse magnetization amplitude is always smaller or significantly smaller than the initial longitudinal magnetization M_0.

The system state can be manipulated at times much smaller than the relaxation times [63, 64]. Let a system be initially characterized by a magnetization M_0. It can be inverted to have the magnetization $-M_0$ (a π-pulse) by applying a field B_1 for the time t_0 given by the relation $\Omega t_0 = \pi$. The system returns to the initial state after the same period of field action, i.e., after the time $2t_0$ (a 2π-pulse). Also worthy of mention is the $\pi/2$-pulse because for some time after its action, the system has zero longitudinal magnetization, i.e., an equality of energy level populations. Instead, a transverse magnetization or energy-state coherence is induced. By combining pulse sequences, it is possible to invert time evolution of the system driven by nonuniform broadening (the spin echo effect).

3.4 Mechanisms of magnetic moment relaxation

The first theory of spin–lattice relaxation was suggested by the German physicist Waller in 1932 [65] to explain relaxation of the electron magnetization in solids. It is equally applicable to nuclear magnetization. According to this theory, thermal oscillations of neighboring magnetic moments create a local alternating magnetic field. Its frequency spectrum contains a resonant frequency component that causes transitions in exactly the same way as an external radiofrequency field does. The probability of such transitions is proportional to the square of matrix elements of the moment projection operators and to the squared amplitude of the radiofrequency field. The following relaxation mechanisms in gaseous media are distinguished.

3.4.1 Nonuniformity of the external magnetic field. Chaotic movements of an atom in a nonuniform magnetic field result in modulation of the local magnetic field acting on the atom (in analogy with the processes considered in the theory of spin–lattice relaxation), with the rate of local field changes being equal to the field gradient times the average atomic velocity.

3.4.2 Spin-exchange processes. In spin-exchange processes, projections of two spin systems change simultaneously as they collide with each other, with the conservation of the total angular momentum. These processes are responsible for the decreased lifetimes of the corresponding states and consequently for the broadening of energy levels. Moreover, spin-exchange processes lead to coherence breakup and thereby

cut short the transverse relaxation time:

$$T_2^{-1} = nv\sigma_{ex}\,, \tag{28}$$

where n is the atomic density, v is the mean thermal atomic velocity, and σ_{ex} is the cross section of the spin-exchange interaction (for potassium, $\sigma_{ex} \approx 3 \times 10^{-14}$ cm^2). However, the effect of the spin-exchange interaction on the transverse relaxation time can be practically excluded under certain conditions, e.g., at a very high atomic density and in very weak magnetic fields [66, 67].

3.4.3 Broadening by a radiofrequency field. The radiofrequency field typically used in magnetic resonance studies causes broadening of the observed resonance line. In the theory of magnetic resonance, this broadening is treated as a manifestation of the saturation effect. The contribution of the radiofrequency broadening is given by the term $\omega_1^2 T_1 T_2$ in the solution of Bloch equation (17).

3.4.4 Relaxation via wall collisions. Collisions with cell walls are important when the atom mean free path is comparable with the cell size. The order of magnitude of this phenomenon can be estimated by dividing the cell diameter d by the mean atomic velocity $\langle v\rangle$:

$$T_1 = \frac{d}{\sqrt{8kT/\pi M}}\,. \tag{29}$$

In the case of potassium atoms within a cell 5 cm in diameter at 50 °C, formula (29) gives a relaxation time of the order of $\sim 1.4 \times 10^{-4}$ s, whereas the characteristic velocity of optical pumping is 10^{-1} s.

A variety of coating materials (paraffins and silicon organic compounds) are used to reduce wall relaxation. Relaxation of optically oriented rubidium atoms on coated walls was investigated in [68–70]. These authors measured relaxation times with different materials and showed that interactions responsible for relaxation during collisions involve hydrogen atoms present in the coating. With the electron paramagnetism of hydrogen atoms compensated by chemical bonds, the leading role belongs to nuclear magnetism; in other words, the relaxation is due to the dipole interaction with the hydrogen nuclear moment. Another component of relaxation depending on the spin–orbital interaction was discovered in experiments where usual paraffin was replaced with deuterated paraffin. Investigations of the relaxation mechanisms in alkali metals, e.g., potassium, were continued in [20, 71–73] in the group headed by E B Aleksandrov. Experiments with cells with a compartment containing a potassium metal droplet confirmed the validity of expression (29) at relatively low temperatures (< 50 °C). Relaxation with the irreversible loss of alkaline atoms on the walls becomes predominant at higher temperatures. This process, studied in specially designed cells, was more pronounced for potassium than for rubidium.

3.4.5 Relaxation in collisions with buffer gas atoms. Relaxation during collisions with buffer gas atoms was thoroughly studied in Refs [74–76]. As noted above, the effect of relaxation slowdown on the walls of a cell containing a buffer gas was accidentally discovered in early optical pumping experiments. The relaxation time in a buffer gas can be calculated by solving the diffusion equation

$$\frac{\partial N}{\partial t} = D\nabla^2 N - kN\,, \tag{30}$$

where D is the diffusion coefficient, $k = W\sigma\langle v\rangle n$ is the probability of atomic disorientation in collisions with buffer gas molecules, σ is the effective collision cross section, $\langle v\rangle$ is the mean relative speed of oriented atoms and molecules of the buffer gas, n is the gas density, and W is the probability of atomic disorientation during collisions.

Solving (30) using the Fourier method [25] under the assumption of the complete wall relaxation gives the following expression in the case of a spherical cell after higher harmonics are disregarded:

$$T_1 = \left[\left(\frac{\pi}{R}\right)^2 D + W\sigma\langle v\rangle n\right]^{-1}. \tag{31}$$

The diffusion coefficient decreases and the atomic density increases with increasing the pressure. Accordingly, the maximum relaxation time in each cell is reached at a certain buffer gas pressure. The probability of disorientation W in collisions of oriented atoms with buffer gas atoms strongly depends on the atomic number of the inert gas. This dependence can be expressed by the empirical formula $W = wZ^3$, where Z is the atomic number of the inert gas and w is a constant coefficient.

The presence of a buffer gas in the cell causes shifts in the resonance frequency of hyperfine transitions. Detailed studies of these shifts in different buffer gases undertaken in [77–79], as well as in [80, 81], with a view to minimizing shifts of the $0-0$ transition in quantum frequency standard schemes, demonstrated that the resonant frequency is a linear function of the buffer gas pressure. Light gases (hydrogen, helium, nitrogen, neon) cause a shift toward higher frequencies, whereas heavy ones (argon, krypton, xenon) diminish the resonant frequency. The choice of an adequate gas mixture allows eliminating the frequency shift, even if at a strictly constant gas temperature and partial pressure.

3.4.6 Relaxation induced by pumping light. The very first experiments on optical orientation of atoms showed that magnetic resonance lines broaden with an increasing intensity of resonance radiation incident on the cell [82]. This phenomenon occurs because pumping causes mediated transitions (through transitions into excited states and spontaneous emission) between Zeeman sublevels of the ground state, with the rate proportional to the light intensity. In a work devoted to the quantum theory of the optical pumping cycle [83], the interaction between an atomic ensemble and the radiation field was described in terms of the density matrix formalism. For this, the interaction with light was introduced into Eqn (21) in the form of relaxation and shift components. As expected, the broadening of the line at a given pump light spectral composition and its shift relative to the resonance line spectral contour in the case of an asymmetric pumping radiation spectral profile proved directly proportional to the pumping intensity.

3.4.7 Total width of the magnetic resonance line. The width of the magnetic resonance (disregarding broadening by an alternating magnetic field) in a paraffin-coated cell with a

side-arm containing a reserve metal volume can be represented as the sum of several constituents:

$$\Gamma = \underbrace{\left[\underbrace{(\Gamma_{\rm wall} + \Gamma_{\rm hole})}_{\Gamma_0} + \Gamma_{\rm coll}\right]}_{\Gamma_{\rm d}} + \Gamma_{\rm light}\,. \tag{32}$$

Here, $\Gamma_{\rm wall} = C_{\rm w}/\tau_{\rm fl}$ is the contribution of wall relaxation, where $C_{\rm w} = C_{\rm w}(T)$ is the probability of electron spin relaxation in a collision with the coating, $\tau_{\rm fl} = \langle l_{\rm fl}\rangle/\langle v\rangle$ is the mean time of flight between the walls, and $\langle l_{\rm fl}\rangle$ is the mean path length between wall collisions. For a spherical cell with a diameter d, $\langle l_{\rm fl}\rangle = k_{\rm form} d$ and $k_{\rm form} \approx 0.7$; for a cylindrical cell with a diameter D and length $L = lD$ $(l > 1)$, $\langle l_{\rm fl}\rangle = k_{\rm form}\sqrt{DL}$ and $k_{\rm form} \approx 0.5$; $\langle v\rangle = \sqrt{8RT/(\pi M)}$ is the mean atom velocity, T is the temperature, M is the molar mass, R is the universal gas constant, and $\Gamma_{\rm hole}$ is the absorption rate of polarized atoms in the side arm. In the simplest case where this reservoir is separated from the cell by a diaphragm with an area s, $\Gamma_{\rm hole} = s/(S\tau_{\rm fl})$, where S is the area of the inner cell surface; $\Gamma_{\rm coll}$ is the line broadening due to atom–atom collisions (*spin-exchange* or *collisional* broadening) proportional to the atomic vapor concentration n: $\Gamma_{\rm coll} = \sigma_{\rm ex} n\langle v_{\rm rel}\rangle$, where $\sigma_{\rm ex}$ is the cross section of the spin-exchange process; $\langle v_{\rm rel}\rangle = \sqrt{2}\,\langle v\rangle$ is the relative velocity of colliding particles; and $\Gamma_{\rm light}$ is light-induced broadening proportional to the pumping light intensity $I_{\rm ph}$.

The square brackets in (32) are introduced to group terms of a similar nature. That is, the first three terms denote the *dark* width of the line, $\Gamma_{\rm d} = \Gamma_{\rm wall} + \Gamma_{\rm hole} + \Gamma_{\rm coll}$. The first two terms in (32) are determined by the cell design and coating quality. This part of the width (*intrinsic resonance width in the cell*), $\Gamma_0 = \Gamma_{\rm wall} + \Gamma_{\rm hole}$, can be measured by extrapolating the width Γ to a zero pumping light intensity and zero atomic concentration:

$$\Gamma_0 = k_{\rm R}\,\frac{\langle v\rangle}{\sqrt{l}\,D}\,,\qquad k_{\rm R} = \frac{1}{k_{\rm form}}\left[C_{\rm w}(T) + \frac{s}{S}\right]. \tag{33}$$

(Here and hereinafter, to equations for a spherical cell of a diameter d can be obtained by replacing $D \to d$, $l = 1$.)

Relaxation due to the departure of atoms into the metal-containing reservoir depends on the size of the diaphragm: it being small, the influence of the atomic absorption inside the reservoir on the relaxation rate can be neglected and $k_{\rm R} \approx k_{\rm form} C_{\rm w}(T)$. Under these conditions, the resonance eigenwidth in the cell is inversely proportional to its diameter:

$$\Gamma_0 = k_{\rm R}\,\frac{\langle v\rangle}{\sqrt{l}\,D} = \frac{C_{\rm w}(T)}{k_{\rm form}}\,\frac{\langle v\rangle}{\sqrt{l}\,D}\,. \tag{34}$$

It is shown in Section 4 that line broadening by pumping light (i.e., light broadening) makes a crucial contribution to the linewidth and is therefore a key factor determining the accuracy of magnetic field measurements. This means that optimization of the pumping light intensity is mandatory for improving the overall efficiency of metrological instruments.

4. Applications of optical pumping and double resonance in magnetometry

Quantum magnetometers can be categorized into several types based on the mode of magnetic resonance detection. The following classification is relevant for the discussion in what follows:

(a) instruments in which a quantity proportional to the longitudinal component of the magnetic moment serves as a signal (M_z-signal). They are exemplified by low-speed, highly accurate M_z-magnetometers;

(b) quick-response M_x-magnetometers — instruments detecting the phase of the oscillating transverse component of the magnetic moment.

4.1 Basic metrological characteristics of quantum magnetometric devices

Both *accuracy* and *variational sensitivity* (or *resolving power*) of instruments of either type are basically limited by the parameters of a magnetic resonance such as symmetry, the resonance linewidth and shift, and the signal/noise ratio.

Variational sensitivity of a magnetometer in a stable field is characterized by the dispersion σ_τ of its readings averaged over a given interval T for a given time τ of a single measurement ($T \gg \tau$):

$$\sigma_\tau^2 = \left\langle B^2(t,\tau) - \langle B_T^2\rangle\right\rangle, \tag{35}$$

where $B(t,\tau)$ is the current reading at an instant t and $\langle B_T\rangle$ is the averaged reading for a time T. It is assumed that the readings obey the Gaussian statistics; measurements obtained for a time $T \geqslant 20\tau$ are considered reliable. However, the sensitivity at different measuring times depends on a variety of factors characterized by different statistics; therefore, the sensitivity calculated by formula (35) does not comprehensively characterize the measurement over the entire time range. The time dependence of sensitivity is usually described in terms of the *Allan diagram* [84] depicting the dependence of the *Allan deviation* $\sigma_{\rm A}(\tau)$ *or the Allan variance* $\sigma_{\rm A}^2(\tau)$ over the measurement time:

$$\sigma_{\rm A}^2(\tau) = \frac{1}{2}\left\langle \big(B_{i+1}(\tau) - B_i(\tau)\big)^2\right\rangle = \frac{1}{2(n-1)}\sum_i \big(B_{i+1}(\tau) - B_i(\tau)\big)^2, \tag{36}$$

where $B_i(\tau)$ represents the results of successive measurements within adjacent time intervals averaged over the time τ. Importantly, in the case of the normal distribution of the results, the Allan variance coincides with the standard one in (35).

The threshold variational sensitivity (i.e., limited only by fundamental physical causes) can be derived from the minimal magnetic field variation that can in principle be detected by a magnetometer for a time τ. This variation may be expressed as

$$\delta B_{\rm min} = \frac{1}{\gamma}\,\frac{N}{\left({\rm d}S(\omega)/{\rm d}\omega\right)\big|_{\Delta\omega = 0}} = \frac{k_{\rm F}}{\gamma}\,\frac{N\Gamma_{\rm full}}{S}\,, \tag{37}$$

where γ is the gyromagnetic ratio, $\Delta\omega = \omega_0 - \omega$, ω_0 is the magnetic resonance frequency, $k_{\rm F}(\approx 1)$ is the resonance form factor, $\Gamma_{\rm full}$ is the total resonance linewidth (taking account of all broadening factors), N is the mean-square noise level

resulting from averaging over the same time τ, S is the signal amplitude at the maximum, and $\mathrm{d}S/\mathrm{d}\omega\big|_{\Delta\omega=0} = (1/k_\mathrm{F})S/\Gamma_\mathrm{full}$ is the resonance signal slope.

Of all possible types of noise in the optical pumping and magnetic resonance detection paradigm, only two of a quantum nature are intractable in principle: these are shot noise of light and quantum noise of an atomic ensemble. However, the mean number of photons detected per unit time $\langle N_\mathrm{ph}\rangle$ in standard pumping schemes is much greater than the number of atoms interacting with light $\langle N_\mathrm{at}\rangle$. Therefore, the noise entering (37) is determined by shot fluctuations of the detected light, which in turn obey the Poisson statistics:

$$P\big[k = n(t+\tau) - n(t)\big] = \frac{\exp\big(-\langle N_\mathrm{ph}\rangle\tau\big)\big(\langle N_\mathrm{ph}\rangle\tau\big)^k}{k!}, \quad k = 0, 1, 2, \ldots, \tag{38}$$

where $P[k]$ is the probability of incidence of k photons on the photodetector for a time τ and $\langle N_\mathrm{ph}\rangle$ is the mean number of photons per unit time.

For a large number $\langle N_\mathrm{ph}\rangle$ of photons incident on the photodetector, this statistics tends to the normal distribution or the Gaussian statistics with $\sigma^2 = \langle N_\mathrm{ph}\rangle$ corresponding to the photocurrent *white noise* I_ph:

$$(\Delta I_\mathrm{ph})^2 = 2e\langle I_\mathrm{ph}\rangle\Delta f. \tag{39}$$

In this case, i.e., when the condition of shot noise dominance over all other noises is satisfied, the minimally measured field variation for a time τ is written as

$$\delta B_\mathrm{min}^\mathrm{light} = \frac{k_\mathrm{F}}{\gamma}\frac{\rho_\mathrm{N}\Gamma}{S}\sqrt{\Delta f} = \frac{1}{Q}\sqrt{\Delta f} = \frac{1}{Q}\frac{1}{\sqrt{2\pi\tau}}, \tag{40}$$

where ρ_N is the shot noise spectral density, $Q = (\gamma/2\pi k)S/(\Gamma_\mathrm{full}\,\rho_\mathrm{N})$ is the resonance quality factor (or Q factor) [85], and Δf is the frequency band corresponding to the measurement time τ. Strictly speaking, the ratio $\Delta f/\tau$ depends on the instrument function of the averaging device. Here, $\tau = 1/2\pi\Delta f$.

Formula (40) holds for the majority of quantum optical magnetometers in which the number of photons in the probe beam interacting with atoms per unit time is small compared with the total number of photons in the beam, and light noise predominates. However, certain situations are dominated by *atomic quantum noise* as the principal factor limiting the sensitivity of the quantum magnetometer:

$$\delta B_\mathrm{min}^\mathrm{at} = \frac{1}{\gamma}\frac{1}{\sqrt{\langle N_\mathrm{at}\rangle T_2\tau}}, \tag{41}$$

where T_2 is the transverse relaxation time and $\langle N_\mathrm{at}\rangle$ is the number of atoms.

Expression (41) is obtained under the assumption [17] that measurement of the precession phase of an individual atom for a time τ is associated with an uncertainty of 1 rad. It can be just as well derived from the relation of the uncertainty of energy measurement for a finite time interval.

Atomic noise may be significant in different situations, first and foremost in dense media where an almost 100% efficiency of optical detection is achieved. Moreover, atomic noise can be expected to dominate in schemes with high-efficiency detection of a luminescent signal (instead of the pumping light absorption signal most frequently used in current practice).

As follows from (37), narrow atomic resonances are especially attractive for quantum magnetometry. However, their intrinsic inertia creates an inconvenience. To find the resonance center from the absorption maximum (as in M_z-schemes), it is necessary to introduce a resonance frequency modulation that cannot be too fast because its own frequency should be consistent with the resonance width. Furthermore, the rate of population changes in the system is limited by the longitudinal relaxation time. On the other hand, the precession frequency of the atomic system can be modified immediately by a magnetic field, and its measurement (as in M_x-schemes) yields a noninertial response.

There is one more consideration in the general case that undermines the advantage of using narrow resonance lines. The fact is, the operational speed of any magnetometer is limited by the fundamental uncertainty of the measurement of a noise-containing harmonic signal frequency within a given time interval. The expression for the lower limit of the error in the measurement of an arbitrary quantity containing a stochastic component is called the Cramer–Rao relation (from the Cramer–Rao lower bound, CRLB) [86]. The expression for the lower accuracy limit in the measurement of a signal containing an additive component in the form of white noise is proposed in Ref. [87]. The operational speed of an M_x-magnetometer is not limited by the resonance linewidth. However, this assertion holds only if the measurement time is not considerably smaller than the reverse linewidth $1/\Gamma$; further reduction of the measurement time leads not to a square root decrease in the sensitivity with the bandwidth but to a linear one or (in the limit) to the one expressed by the law $\delta B \sim T^{-3/2}$. Moreover, at high measurement times that characterize both the *accuracy* and *stability* of a magnetometer, various drifts and agings statistically described by dependences $\sigma_\mathrm{A}(\tau) \sim \tau^{1/2}$, $\sigma_\mathrm{A}(\tau) \sim \tau$, and so on become predominant (see below).

One more important metrological characteristic of magnetometric devices, besides the *variational sensitivity* and *operational speed,* is the *absolute accuracy* or the accuracy with which the induction of the field being measured can be expressed via fundamental constants. For example, the limiting absolute accuracy of a K-magnetometer depends on the errors in the measurement of the quantities g_J, μ_B, and h: $\Delta g_J/g_J = 1.2\times10^{-7}$, $\Delta\mu_\mathrm{B}/\mu_\mathrm{B} = 8.6\times10^{-8}$, and $\Delta h/h = 1.6\times10^{-7}$ [88]. Consequently, the ultimate absolute accuracy of a K-magnetometer in the typical Earth magnetic field (EMF) of 50 μT can be roughly 10 pT. Also, errors in magnetic resonance frequency measurements with a K-magnetometer can be reduced to 10 pT. Such are the characteristic values of shifts and errors in the measurement of the magnetic resonance frequency in the potassium spectrum with the magnetic resonance linewidth 1 nT.

Comparison of Allan diagrams of different magnetometric devices indicates that they are characterized (similarly to frequency references) by the measurement time τ_0 at which the decrease in the dispersion $\sigma_\mathrm{A}(\tau) \sim \tau^{-1/2}$ inherent in shot noise is followed by a flat part or an increase. Such behavior is due to parametric shifts of the resonance line itself and to errors in the detection of its position. Variations over the section $\tau > \tau_0$ determine the measurement accuracy of selected parameters, such as *long-term stability*, i.e., variations in reading error at time scales of $10^3 - 10^6$ s.

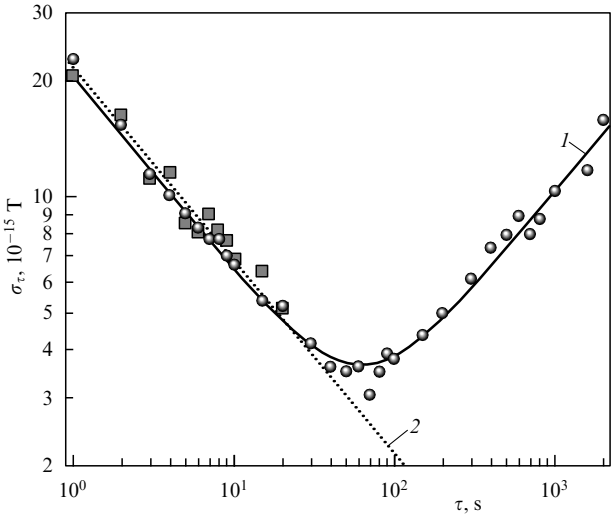

Figure 5. Allan variance (curve *1*) of the readings of a rubidium (^{87}Rb) magnetometer calculated from the experimentally measured difference between readings of single-cell ^{85}Rb and ^{87}Rb magnetometers. Resolving power (*2*) of an ^{87}Rb channel computed from the magnetic resonance *Q*-factor.

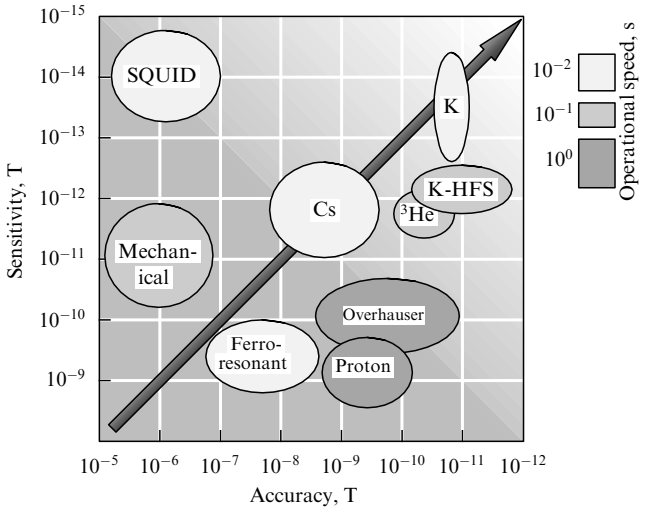

Figure 6. Classification of magnetometric instruments by major metrological parameters.

We note that the measurement of intrinsic noise characteristics of a magnetometric instrument encounters serious difficulties because it requires the elimination of the contribution of magnetic field variations at the level of 10^{-15} T. It is impossible to stabilize the field or compensate its variations with such an accuracy, at least as far as geomagnetic fields are concerned. Results of a direct measurement of the OPQM accuracy at the level of 10^{-14} T Hz$^{-1/2}$ in a nonzero magnetic field are presented in Ref. [89]. In this experiment, the effect of variations in the magnetic field gradient was neutralized by using two magnetometers with a common cell containing vapors of rubidium isotopes, ^{85}Rb and ^{87}Rb, and measuring the difference between their readings. This approach permitted obviating the major problem of comparing the readings of two sensors: under usual conditions, they are spatially separated, and the difference between their readings depends on fluctuations of the magnetic field inhomogeneities. In the case of a cell containing the vapor of two substances, the sensors are coincident.

Figure 5 shows a result of such measurement in the form of an Allan diagram and compares it with magnetometer noises estimated from the magnetic resonance *Q*-factor. Excellent agreement between the data gives additional evidence of the validity of assessment of the magnetometer resolving power based on the magnetic resonance quality factor.

Other important metrological characteristics of magnetometers include the *reproducibility of readings*, i.e., their variation from one switch-on to another, and various parametric dependences, e.g., the *orientational error* or the dependence of readings on the sensor orientation with respect to the field vector. Most of these parameters are in turn related to the characteristics of the magnetometer such as the stability of the light spectral composition of its lamp and the cell temperature, the aging rate of the cell coating, etc. Clearly, the totality of these random factors are not as readily amenable to formalization as the ultimate sensitivity of the instrument. The severity of errors due to all these factors is proportional to the resonance width Γ.

It follows from the above that the parameters of a magnetometric device must be optimized for a concrete purpose. For example, reduction of the resonance width is a priority for applications requiring high measurement accuracy but not high operational speed at small times ($< T_2$).

Figure 6 gives an example of the classification of modular magnetometric instruments by the main metrological characteristics, such as the short-term sensitivity, accuracy, and operational speed. The arrow shows the generalized vector of the magnetometric instrument development. The classification is neither comprehensive nor definitive, because a direct assessment of the parameters of high-precision instruments is impracticable when they surpass the respective parameters of reference devices. Moreover, some of the magnetometers listed in Fig. 6 are designed to measure quantities other than the modulus of the magnetic field induction. For example, mechanical and ferro-resonance magnetometers (*fluxgates*) can measure the field modulus only by measuring three components of the magnetic induction vector, whereas SQUIDs measure increments of the magnetic flux through a contour.

Researchers in different countries do not keep to unified methods of measuring the parameters of magnetometers, and there is no universally accepted system of such parameters. Suffice it to say that estimates of the SQUID short-term sensitivity vary from 10^{-15} T to 10^{-12} T, while data on their accuracy are virtually unavailable. Also, it is known that SQUIDs are fairly sensitive at high frequencies, but noises increase with decreasing the frequency. However, the diagram does not reflect this situation. The area occupied by the Cs magnetometer in the diagram should be enlarged several-fold based on the wide scope of applications of this instrument (including its high-precision many-cell modifications and miniature commercial variants).

Finally, manufacturers' specifications of commercial magnetometric devices are frequently at variance with more humble estimates of their characteristics in independent tests. This assertion refers first and foremost to the instruments of small private western companies. In other words, Fig. 6 is designed to give only a general idea of the current state of the art in quantum magnetometry.

4.2 Optimization of the quality factor of a magnetic M_x-resonance under optical pumping conditions

Expressions for the dependence of the signal amplitude on the pumping light intensity were first proposed by Dehmelt [90, 91], and Bloom [92] was the first to point out the necessity of Q-factor optimization based on light intensity measurements. As shown in Ref. [93] in application to the M_z-signal of a quantum frequency discriminator, the light intensity $I_{\rm opt}$ ensuring its broadening by a factor of 3–4 is optimal when technical noises are suppressed strongly enough for the shot noise of light to become dominant. Because only one beam is used in the standard OPQM for both pumping and recording, its propagation angle with respect to the magnetic field direction must also be optimized; the same is true of the angle between the vector of the alternating magnetic field (radiofield) and the direction of the pumping beam. These two problems were resolved for a simulated two-level system in Ref. [92], where the optimal angle θ between the vector of the alternating magnetic field and the beam direction was found to be 45° and the angular dependence of the signal maximum $S(\theta)$ varied only insignificantly with changes in the radiofield strength [$S(\theta) \sim \sin\theta\cos\theta$ if this effect is disregarded]. The alternating magnetic field B_1 should be parallel to the pumping beam; otherwise, the axial symmetry of the system is broken and the signal becomes dependent on one more angle. It was shown in Ref. [92] that such a configuration leads to a 90° phase shift between the light modulation signal and the radiofield, which must be compensated with an accuracy determined by the resonance linewidth and requirements on the accuracy of field measurement.

An exact solution of the problem of the M_x-resonance in a many-level system inside a paraffin-coated cell is a rather difficult task (see, e.g., Ref. [94]). It requires taking into account the dependence of absorption, collisional, and light broadening on the degree of matter polarization, which is in turn determined by pumping conditions. In the case of a paraffin-coated cell in which 'intermixing' of the excited levels is negligibly small, such a problem may have only a numerical solution. However, a relatively simple model proposed in [95] provides correct quantitative predictions. The model is based on the following approximations:

(1) The magnetic resonance is described by Bloch equations [1] for a two-level system.

(2) The spin-exchange broadening of the resonance line is independent of the degree of the working agent polarization.

(3) A large atomic lifetime $\tau_{\rm fl}$ in the cell compared with the time of flight between the walls results in an overall effective averaging of the pumping light intensity and a uniform distribution of the population of each level across the cell. For the same reason, all atoms in the cell are efficiently pumped with a monochromatic radiation tuned to the center of the Doppler absorption line.

(4) The pumping spectrum width is small in comparison with that of the absorption resonance line (laser pumping). In the case of a wide-spectrum pumping (lamp), such an approximation leads to quantitative discrepancies between simulation and experiment at large optical thicknesses ($x \gg 1$).

The dependence of the magnetic resonance quality factor (optimized relative to the driving field amplitude) on the pumping intensity within a unit frequency band is given by

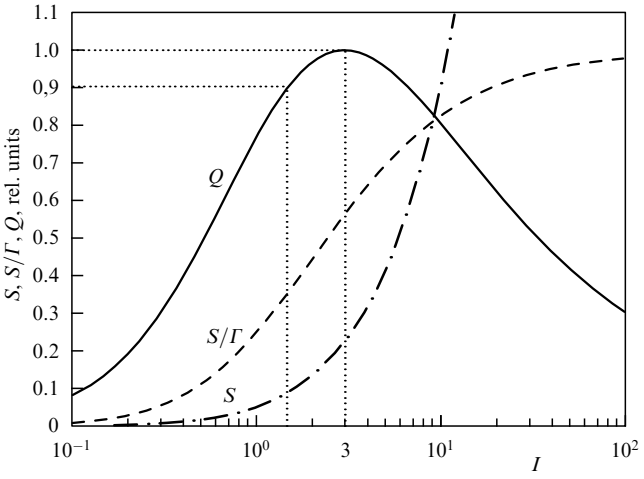

Figure 7. Plots of the signal S, the S/Γ slope, and the Q factor of magnetic resonance vs the light broadening $I = \Gamma_{\rm light}/\Gamma_{\rm d}$.

$$Q = \gamma K \frac{V^{1/2}}{\left(\sqrt{2}\,\sigma_{\rm ex}\langle v\rangle\right)^{1/2}} \frac{I^{3/2}}{(1+I)^2} \times \frac{x}{\left[\exp(x)-1\right]^{1/2}\left[1+1/(\alpha x)\right]^{1/2}}, \qquad (42)$$

where $I = \Gamma_{\rm light}/\Gamma_{\rm d}$ is the dimensionless pumping intensity equaling the light-broadening/dark-width ratio, $x = \kappa L = k_v n L$ is the optical thickness of the cell, $V = (\pi/4)d^2 L$ is the cell volume, $\alpha = (\Gamma_{\rm coll}/\Gamma_0)/x$ is the coefficient describing the cell properties (α is inversely proportional to cell diameter d and the resonance eigenwidth Γ_0), $\alpha = k_\alpha/(d\Gamma_0)$, $K = \sqrt{\psi k_{\rm det}}\, k_{\rm pump} k_{\rm read}$ is the coefficient characterizing the efficiency of pumping and detection of the M_x-resonance, $k_{\rm pump}$ is the optical pumping efficiency, $k_{\rm read}$ is the efficiency of the atomic polarization signal 'readout' by the detecting light, and $k_{\rm det}$ is the quantum yield of the photodetector.

The dependences of the signal, slope, and Q factor on the pumping intensity presented in Fig. 7 show that the quality factor reaches a maximum at $I_{\rm opt} = 3$ (in agreement with the fourfold broadening of the resonance line). However, all light and related parametric shifts of the resonance line (hence, their variations) are proportional to the pumping intensity. Therefore, the working intensity to be chosen at the sloping portion of this dependence should be lower than $I_{\rm opt}$. For example, reduction of the intensity by a factor of 2 corresponds to less than a 10% decrease in the Q factor.

Interestingly, the signal slope S/Γ at given I and x does not directly depend on the resonance linewidth, i.e., the coating properties. The entire linewidth dependence of the Q factor is determined by the contribution of the noise term; that is, a broad-line pumping requires an enhancement of its power, which leads to an increase in the level of light shot noises.

Expression (42) can be rewritten as

$$Q(\alpha, x, D, l, I) = \gamma K Q_1(V)\, Q_2(I)\, Q_3(\alpha, x). \qquad (43)$$

Only the last factor, $Q_3(\alpha, x)$, depends on the cell optical thickness x. Evidently, the Q-factor optimum position $x_{\rm opt}$ across the cell optical thickness (hence, across vapor concentration) is determined by the parameter α alone. The value

of $x_{\rm opt}$ can be approximated by the dependence

$$x_{\rm opt} \approx 1.59 + 1.23\left(1+\frac{\alpha}{2}\right)^{-0.91}. \qquad (44)$$

The optimal values are $x_{\rm opt} = 1.59-2.82$.

It is important that the parameter α enters (42) only in the combination $(1+1/\alpha x)^{-1/2}$ and for $\alpha x \gg 1$, as is almost always the case in cells with a small intrinsic width. This allows neglecting the dependence of the Q factor on α, and hence on the cell coating properties. This inference has a simple physical justification; the quality factor is primarily determined by absorption within the cell, which imposes a stringent limitation on its optical width ($x_{\rm opt} \geqslant 1.59$) and thereby on the spin-exchange broadening. For ^{39}K at $T = 300$ K and the D_1-line pumping,

$$\frac{\Gamma_{\rm coll}^{\rm opt}}{2\pi} L > 16.4 \text{ Hz cm}, \qquad (45)$$

and for a cell 5 cm in diameter,

$$\frac{\Gamma_{\rm coll}^{\rm opt}}{2\pi} = 3.3 \text{ Hz}. \qquad (46)$$

We note that the larger optimal linewidth $\Gamma_{\rm d}$ (compared with that in [93]) requires the greater light broadening $\Gamma_{\rm light}$ to attain the same intensity $I_{\rm opt}$. Therefore, spin-exchange broadening in the case of optimal optical thickness of the cell neutralizes the advantages of using hyperfine lines in coated cells.

Expressions (37) and (43) allow estimating the maximally attainable sensitivity $\delta B_{\rm min}$ of the quantum M_x-sensor: at an optimal I and x, the product $Q_{2\,\max} Q_{3\,\max} = 0.325 \times 0.805 = 0.262$. Therefore, at the optimal pumping parameters,

$$Q_{\max} = K'_{\rm opt}(\psi k_{\rm det})^{1/2} V^{1/2} \left[\text{T}^{-1}\ \text{Hz}^{1/2}\right], \qquad (47)$$

where $K'_{\rm opt} = 1.84 \times 10^{13}$ cm$^{-3/2}$ for potassium and $K'_{\rm opt} = 1.42 \times 10^{12}$ cm$^{-3/2}$ for cesium. Under the experimental conditions described in Ref. [15] with the cell diameter 15 cm and the detection coefficient $k_{\rm det} = 0.35$ (here, $k_{\rm det}$ contains the filling coefficient of the multifiber lightguide), $\delta B_{\rm min} = 1.6 \times 10^{-15}$ T Hz$^{-1/2}$, which is confirmed by the results of measurements in Ref. [15].

The physical meaning of the coefficients in (43) becomes clear if Q_1 is expressed in terms of the number of atoms in the cell:

$$Q_1(V) = \left(\frac{N_{\rm at}}{\Gamma_{\rm coll}}\right)^{1/2}. \qquad (48)$$

As follows from (48), the Q factor is proportional to the square root of the number of atoms in the cell. Up to now, we have assumed that the limiting factor of the sensitivity of a quantum optical-pumping discriminator is the shot noise of the photocurrent. It follows from (41) that the coefficient Q_1 entering (48) is equal (up to $\sqrt{2\pi}$) to the quality factor $Q_{\max}^{\rm at}$ limited by atomic noises; hence,

$$Q(\alpha, x, d, l, I) = \sqrt{2\pi}\, K Q_2(I)\, Q_3(\alpha, l, x)\, Q_{\max}^{\rm at}, \qquad (49)$$

or, at optimal I and x,

$$Q_{\max} \approx \frac{2}{3} K Q_{\max}^{\rm at}. \qquad (50)$$

Hence, the limiting quality factor is determined by quantum atomic noise and the efficiency of optical pumping/resonance detection. For a K-discriminator, $Q_{\max}/Q_{\max}^{\rm at} \approx 0.025$, i.e., the light noise exceeds the quantum atomic noise by one and a half orders of magnitude, because the number of photons interacting with probe beam atoms per unit time is small compared with the total number of photons in the beam.

As noted in Section 4.1, there is one more consideration undermining the advantage of using narrow resonance lines: the operation speed of any quantum magnetometer is limited by the fundamental uncertainty described by the Cramer–Rao relation [86].

The expression for the Cramer–Rao lower bound contains an additive component in the form of white noise as reported in [87]. This uncertainty calculated over the magnetic field B scale can be represented as

$$\delta B_{\rm min}^{\rm meas} = \frac{1}{\gamma}\frac{\sqrt{3}}{\pi}\frac{\rho_{\rm N}}{S}\frac{1}{\tau^{3/2}}. \qquad (51)$$

The dependence $\delta B \sim \tau^{-3/2}$ in (51) can be physically interpreted as follows: the spectrum of a sinusoidal length τ is a bell-shaped function with a contour about $1/\tau$ in width. If white noise is added to this spectrum, the error in the detection of the contour center is proportional to the contour width $1/\tau$ times the noise/signal ratio in the frequency band of the order of $1/\tau$, which is in turn proportional to $\tau^{-1/2}$.

For convenience, Eqn (40) can be rewritten as

$$\delta B_{\rm min}^{\rm light} = \frac{1}{\gamma}\frac{2}{\sqrt{2\pi}}\frac{\rho_{\rm N}}{S}\frac{1}{T_2\sqrt{\tau}}. \qquad (52)$$

For a measurement time $\tau \gg T_2$, the limiting sensitivity of a magnetometer is given by formula (52) and obeys the square-root dependence on time. For $\tau \ll T_2$, the limiting sensitivity decreases with decreasing the measurement time as $\tau^{-3/2}$ in accordance with (51).

We note that the Cramer–Rao limit has a fundamental nature and cannot be overcome in any system, including one that contains no scheme for measuring frequency in an explicit form. Such a scheme is exemplified by a magnetic field stabilizer in which the output frequency of the magnetometer is compared with a given frequency and the difference is directly (i.e., without measurement) converted into a stabilizer coil current.

At time scales of tens of seconds or greater, various slow drifts (usually described by dependences $\sim 1/f$, $\sim 1/f^{1/2}$, and so on) begin to markedly affect readings of the discriminator. Discussion of these effects is beyond the scope of the present review. Suffice it to mention an important feature of quantum discriminators: their drifts at large times cannot be arbitrarily large, being limited by the width of the resonance line. Thus, its narrowing is the key issue in situations requiring high measurement accuracy at large times; in each concrete problem, priority is given to either sensitivity or accuracy.

4.3 Modern quantum magnetometric instruments

4.3.1 Self-generating cesium magnetometer. The history of the self-generating M_x-magnetometer dates back to the works of H Dehmelt [90, 91] published in 1957, who was the first to use a transverse light beam to detect magnetic resonance and show that the light absorption signal can be used to create self-generating systems. Dehmelt's idea was experimentally verified in the same year by Bell and Bloom [96]. The working

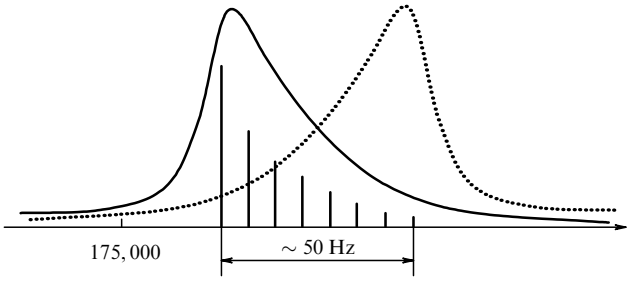

Figure 8. Diagram illustrating the evolvement of asymmetry of the Cs magnetic resonance line in the Earth's magnetic field.

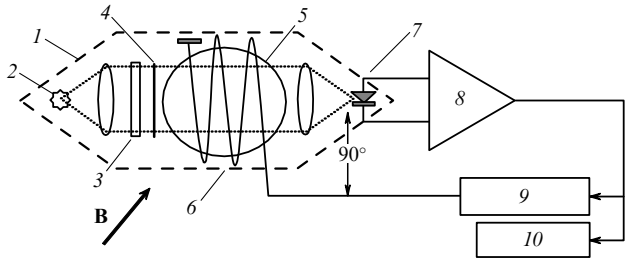

Figure 9. Simplified schematic of the self-generating Cs magnetometer: *1* — sensor, *2* — Cs vapor lamp, *3* — D_1-filter, *4* — circular polarizer, *5* — alkali metal vapor cell, *6* — resonant rf coil, *7* — photodetector, *8* — fotocurrent amplifier, *9* — phase inverter, *10* — frequency meter.

agent in the first self-generating magnetometers was rubidium, which was later replaced with cesium for practical reasons.

The self-generating Cs magnetometer appears to be the simplest and most widely used quantum magnetometer, although cesium has the most complicated structure of the magnetic ground state sublevels. The ground state of ^{133}Cs comprises two hyperfine levels with the total angular momenta $F = 3$ and $F = 4$ subject to respective splitting into 7 and 9 sublevels in a magnetic field. For cesium, the difference between the magnetic resonance frequencies of adjacent magnetic sublevels of one hyperfine level in the Earth's average magnetic field does not exceed 7 Hz. Therefore, many resonances actually blend into a single asymmetric resonance hybrid some 50 Hz in width, roughly corresponding to 15 nT on the magnetic field scale (Fig. 8).

The magnetometer works as a molecular frequency generator with an amplifier in the feedback loop. Light emitted by a Cs lamp is directed at an angle of $45° \pm 15°$ with respect to the measured magnetic field. This light is used for pumping Cs vapor in a paraffin-coated cell (Fig. 9). The same light is used to record the resonance. The amplified signal is transmitted from the photodetector to the rf coil. Noise components of the photosignal trigger a priming signal at the Larmor precession frequency in the external magnetic field. This signal is additionally amplified, phase-shifted, and again transferred to the cell through a feedback loop. Taken together, these events give rise to self-generation at the aggregate resonance frequency in the state $F = 4$ (devices based on this principle are called *spin generators*). The generation frequency is roughly proportional to the strength of the external magnetic field with the proportionality coefficient around 3.5 Hz nT^{-1}. The magnetometer may be operated without a thermostabilization system, Cs vapor pressure at room temperature being close to optimum. Pumping is feasible without light filters (i.e., with a mixture of two resonance lines) in order to simplify the optical scheme of the instrument.

The contribution of various partial resonances strongly depends on many factors, such as the light and radiofield intensity, the direction of the pumping light relative to the direction of the constant field, and the Cs vapor density; all this contributes to the uncertainty of the resonance maximum position as a function of the measured field strength. Consequently, the accuracy of a Cs magnetometer does not typically exceed several nT, which manifests itself in both the irreproducibility of the readings in different runs and in slow drifts of the readings even in an ideally stabilized field.

The so-called orientational shifts of the magnetometer frequency upon a change of the angle between the optical axis and the magnetic field vector are especially undesirable for magnetic prospecting. On the other hand, a resolution of 1 pT Hz$^{-1/2}$ can be reached within a short observation time, $\tau = 10-100$ s, if the magnetometer is fixed in space; at such τ intervals, noises of a Cs magnetometer are determined by shot noises of the photocurrent. The effect of the magnetometer parametric frequency shifts becomes apparent as τ increases. Their slow drifts are diminished by thorough stabilization of the pumping light intensity, the working volume temperature, and the rf field strength.

Orientational shifts and drifts can be controlled by special resonance symmetrization techniques. A configuration for this purpose was proposed by Bloom [92] in 1961 in application to an Rb magnetometer; the idea was to pump a block of two cells in opposite directions and to sum up the two output signals. The result was the effective superposition of two asymmetric contours (see Fig. 8), giving rise to a single wide and quasi-symmetric contour. Such a complication of the construction allowed reducing measurement errors by a factor of 10; this, however, is insufficient for many applications.

Subsequent decades witnessed considerable efforts to reduce systematic errors of Cs magnetometers [97–101]. Of special note among the work to this effect done in this country is that by A N Kozlov and co-workers (Pushkov Institute of Terrestrial Magnetism, Ionosphere and Radiowave Propagation) [102]. Magnetometers with six and more cells were constructed, but even these devices failed to resolve the problem [103] because complete compensation of the shifts is precluded by variations in the difference between partial pressure in individual cells, pumping conditions, etc. Moreover, even small field gradients around a multicell magnetometer serve as additional sources of errors. Attempts to use mobile magnetometers with an active spatial orientation system were undertaken in the USA in the 1960s. These instruments had better characteristics than multicell magnetometers (even if at the expense of being much more costly and complicated), but they were not totally free of errors related to parametric shifts when operated at a broad asymmetric resonance line.

The next step toward improving the absolute accuracy of Cs magnetometers was the development of a sensor having a two-compartment cell pumped by left- and right-hand circularly polarized beams [104]. Such a configuration allows reducing orientational shifts to just several tenths of a nanoTesla because the resonance line remains too wide even when symmetric.

For all that, Cs magnetometers are still the simplest, most reliable, and widely used quantum magnetometric devices,

finding increasingly more extensive application due to the advent of readily available sources of laser pumping for cesium. An example is the cardiogradiometer with Cs-M_x-sensors and laser pumping developed by the group of A Weis at the University of Freiburg (Switzerland). This instrument with a 20×20 mm cell has a sensitivity of 100 fT $\text{Hz}^{-1/2}$ [105].

Cesium magnetometers are widely used in gradientometric systems, both stationary and mounted on terrestrial or aerial carriers [106].

We note that the disadvantages of Cs magnetometers related to the resonance line asymmetry are practically inapparent in magnetic fields not exceeding 10% of the Earth's magnetic field (< 5 μT), in which the Cs-line broadening associated with the quadratic Zeeman splitting is negligibly small. The same authors have recently described [107] a non-self-generating Cs magnetometer with laser pumping having the sensitivity 15 fT $\text{Hz}^{-1/2}$ in a 2 μT field.

4.3.2 Magnetometer utilizing transition in the hyperfine structure (HFS magnetometer). HFS magnetometers are essentially different from the M_x-magnetometer described in Section 4.3.1 (based on the coherence resonance between a pair of magnetic sublevels of a single hyperfine level) in that (1) the magnetic resonance in an HFS magnetometer is excited between magnetic sublevels of different hyperfine levels, and (2) HFS magnetometers detect changes in the longitudinal magnetization component.

The first quantum optical-pumping magnetometer based on the UHF resonance in the HFS of ground state alkali metal atoms (HFS magnetometer) was proposed in the 1970s [108–111]. At first sight, the idea to measure magnetic fields from the field dependence of the transition frequency $F, m_F \Leftrightarrow F+1, m_{F+1}$ seems strange because this frequency contains a very large field-independent term equal to the hyperfine splitting. However, this inconvenience is outweighed by many advantages, both technical and fundamental, over the traditional OPQM design.

First, the Zeeman structure of most HFS transitions is resolved even in superweak fields of the order of 10^{-7} T because g-factors of the lower and upper hyperfine levels of the ground state of alkali metals have opposite signs. This accounts for the ability of HFS magnetometers to operate in the magnetic field range $10^{-7}-10^{-3}$ T.

Second, spectrum-selective (not polarization) pumping is possible with HFS magnetometers. It permits using unpolarized radiation of both resonance D_1- and D_2-lines to simplify and lower the cost of the optical system of magnetometers. In this case, the pumping light can be arbitrarily directed with respect to the magnetic field. Hence, the absence of 'blind zones' that appear during efficacious isotropic pumping only due to the vector character of the UHF field action on the atomic system. Because the wavelength of the UHF transition for Cs and Rb lies in the centimeter range (and in the decimeter range for K), it is possible to form an appropriate UHF field configuartion in the cell to prevent blind zones. Such a device can operate at any angle between the optical pumping axis and the direction of the magnetic field vector.

Third, the systematic errors of such a magnetometer can be reduced to 1 pT by means of the so-called balanced modification to measure transition frequencies between two symmetric pairs of magnetic levels (e.g. $|F=2, m_F=-2\rangle \leftrightarrow |F=1, m_F=-1\rangle$ and $|F=2, m_F=2\rangle \leftrightarrow |F=1, m_F=1\rangle$) (Fig. 10). The resulting information in this scheme is carried by the frequency difference between two HFS transitions. In the case of optical pumping with unpolarized light, this difference is virtually free of light shifts because all magnetic sublevels of a given hyperfine level undergo identical light shifts (as well as 'collisional' ones, which are so critical for gas-cell frequency standards). We note that this difference is given by $f_{\text{HFS}}(B) = 6\gamma B$, where γ is the gyromagnetic ratio. In other words, the sensitivity of such a balanced magnetometer is 6 times that of a magnetometer using a transition between the adjacent magnetic sublevels of a given hyperfine level. The field dependence of the output frequency contains no quadratic term, i.e., it is practically linear because the terms of the dependence $f_{\text{HFS}}(B)$ starting from the cubic one are negligibly small.

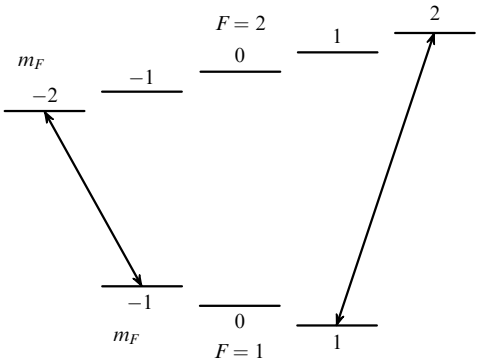

Figure 10. Level diagram of a balanced HFS magnetometer (the distances are not to scale).

Certainly, HFS magnetometers have some disadvantages if compared with traditional OPQMs. First, they are designed to record resonances in populations of magnetic sublevels (M_z-resonances); therefore, they are inferior to M_x-magnetometers in terms of operational speed. Second, they operate in the UHF range and simultaneously measure two transition frequencies, which requires more complicated electronics. The second drawback has been totally eliminated quite recently by using up-to-date methods of frequency synthesis. A perfectly symmetric balanced magnetometer based on single-photon HFS transitions in the ^{87}Rb ground state is described in Ref. [112]; it is characterized by the short-term sensitivity 6.0 pT (mean-square error for 0.1 s). As expected, its sensitivity is limited by UHF tract noises; blind zones were absent.

4.3.3 Nuclear helium magnetometer. The operating principle of a magnetometer using the nuclear spin orientation of helium isotope ^{3}He is expounded in Section 2.4.4. A weak discharge sends ^{3}He atoms into the metastable triplet 2^3S_1 state, where they undergo optical pumping using resonance triplet lines $2^3S_1 \Rightarrow 2^3P_{0,1,2}$ (Fig. 2a). Alkali metal atoms are always pumped in the presence of a buffer gas, e.g., ground-state He atoms. Different triplet components ensure pumping in opposite directions; the pumping becomes impossible if they have identical intensities (as in the case of alkali-atom pumping on both equally intense lines of a resonance doublet). But in reality, these lines always have different intensities, which ensures rather efficacious helium orientation. The pumping efficiency can be enhanced by using an ^{4}He vapor discharge lamp that selectively excites the D_0 line ($2^3S_1-2^3P_0$) of the ^{3}He isotope by virtue of isotopic shift (Fig. 2a). Marked improvement in orientation is achieved by pumping laser radiation resonant with the D_0 line.

Collision of a metastable helium atom with a ground-state He atom gives rise to nuclear polarization amounting to 50%. This process is promoted by the very slow relaxation of magnetized He nuclei poorly adsorbed on the cell walls. (Nuclear spin relaxation time varies from tens of minutes to 10 hours depending on the glass properties. This uncertainty was eliminated after it had been found empirically that a Cs monolayer on any glass surface slows down helium relaxation and prolongs it for days. Practically speaking, relaxation time in these conditions is limited by nonuniformity of the magnetic field.) Helium polarization is detected from pumping light absorption by metastable He atoms.

Interaction with metastable atoms is a source of relaxation of oriented nuclei. To ensure the survival of magnetized He nuclei over the entire lifetime, it is necessary to break the bonds between the nuclei and metastable atoms after maximum polarization is reached, i.e., to cancel the weak discharge generating metastable atoms. This results in the loss of the optical tracking channel for nuclear magnetization. However, the magnitude of such magnetization being very high, it can be monitored directly from its manifestations, such as induction signals from precessing He nuclei.

Nuclear helium magnetometers have not found wide application for several reasons. First, because of their low operational speed; second, they are large and heavy, since heavy induction coils are needed to pick up signals; third, detecting coils are very sensitive to rf noises. Moreover, the magnetometers are highly susceptible to gyroscopic errors due to the low frequency of nuclear precession (a typical gyroscopic error equals the angular rotation frequency divided by gyroscopic ratio γ [113]). The gyroscopic ratio for nuclei is $\gamma/2\pi = 0.032435$ Hz nT^{-1}, and hence rotation with the frequency $(2\pi \times 1/120)$ rad s^{-1} leads to a shift of 0.25 nT.

The advantages of nuclear helium magnetometers include the virtually infinitely narrow line and the ability to operate autonomously in unperturbed conditions within almost 24 hours after the completion of pumping.

Under appropriate conditions, an inductive feedback between the coils and the atomic ensemble may give rise to stationary generation at the Larmor frequency. An instrument based on this principle is called the helium Zeeman maser [114–116].

Nuclear helium magnetometers are most actively developed in France (Laboratoire CIRIL–ISMRA, Caen). A magnetometer using semiconductor laser pumping is described in Ref. [117]. An equilibrium orientation of 13% is reached in this device roughly within 10 min at the pumping power 5 mW and helium pressure 3.5 Torr. As soon as pumping is completed, nuclear magnetization turns across the magnetic field by a $\pi/2$ pulse of the resonance radiofield. The induction signal is detected by coils of 2200 turns each; the signal has an amplitude of a few microvolts. The effect of the coils on the atomic ensemble is reduced by an amplifier with a high input impedance (10^{12} Ω). Such a weak interaction with the coils accounts for signal attenuation within 200 min. The relaxation time in the absence of the coil effect is roughly 24 h. The estimated sensitivity of the magnetometer is 50 pT in a bandwidth of 70 Hz. The gyroscopic sensitivity is 0.5 rpm.

The ^{199}Hg and ^{201}Hg isotopes, besides ^{3}He, are used in nuclear magnetometers with optical pumping [118].

4.3.4 Optical-pumping ^{4}He-magnetometer. Optical pumping of ^{4}He atoms in the metastable 2^3S_1 state first described in 1960 [119] gave impetus to the development of ^{4}He magnetometers [120–122]. The operating principle of these instruments consists of exciting atoms into the metastable state, direct optical pumping (polarization) of 2^3S_1-metastable helium atoms, exciting an M_z-resonance, and the optical detection of the M_z-signal. The resonance in the metastable Zeeman structure is induced either by application of a resonant alternating magnetic field or (for laser pumping of helium) by the amplitude or frequency modulation of laser light (parametric resonance).

The ^{4}He magnetometer does not need sensor thermostatting and is therefore ready to operate as soon as it is switched on; this feature constitutes an indisputable advantage of instruments of this class. A relatively wide magnetic resonance line (≈ 1000 Hz) accounts for the rather high operational speed in a simple M_z-scheme (M_x-schemes have also been used under laboratory conditions, including parametric excitation of resonance by means of the amplitude or frequency modulation of the pumping laser). An additional advantage is a linear dependence of the resonance frequency on the magnetic field.

Certainly, the large width of the resonance line can be a source of serious systematic errors associated mostly with light shifts. This disadvantage may be obviated by using the pulse pumping technique [123]. Moreover, light shifts can be fully eliminated (at least in theory) in schemes where optical alignment of helium atoms is created by laser pumping of the $2^3S_1 - 2^3P_0$ transition.

In the latest modification of the He-magnetometer with laser pumping of the $2^3S_1 - 2^3P_0$ transition [124], frequency modulation of laser radiation, and optical detection of the signal, the sensitivity 1–4 pT Hz$^{-1/2}$ is achieved. This value is significantly different (by three orders of magnitude) from the one predicted in Ref. [125] (4 fT Hz$^{-1/2}$), the cause of the discrepancy being attributed by the developers (Laboratoire CIRIL–ISMRA) to the excess noise of the pumping laser. This problem is common with laser-pumped magnetometers, in which the signal tends to be destroyed not only by intrinsic noise but also by noise resulting from random modulation of laser light polarization and brought in through optofibers. These noises have an especially pronounced effect on the M_z-signal.

The angular range of the magnetometer in Ref. [124] was extended by using two cells through which the light from a single laser (with orthogonal linear polarizations) was passed to be collected in one photodetector. Such a design permits excluding blind zones without substantially complicating the design due to the use of one pumping source, one amplifier of photocurrent, and one phase locked loop (PLL) circuit.

4.3.5 Alkali–helium magnetometer. The alkali–helium magnetometer uses the effect of spin polarization transition during atomic particle collisions in alkali–helium gas discharge plasma. The most important contribution to its development was made by R A Zhitnikov and co-workers (Ioffe Physical Technical Institute, Russian Academy of Sciences). They experimentally demonstrated and investigated the relation between the probability of Penning ionization during collisions of alkali metal atoms with metastable helium atoms and the mutual orientation of electronic spin angular momenta of the partners. The atomic spin orientation in alkali–helium plasma was shown to affect its electric conductivity. Detailed studies of spin orientation transfer from optically oriented atoms of alkali metals to

alkali–helium plasma products (2^3S_1-metastable He atoms and free electrons) are reported in Refs [45, 127]. An important achievement is the possibility of orienting spin momenta of helium 2^3S_1 atoms in the absence of direct optical pumping with resonance helium light that permits the elimination of large light shifts in the frequency of magnetic resonance excited in the system of Zeeman sublevels of 2^3S_1-state He atoms.

A new type of quantum magnetometric device, He-magnetometers with optical orientation of alkali metal atoms or alkali–helium magnetometers, was proposed in Refs [128, 129]. At present, polarization of helium 2^3S_1 atoms by spin orientation transfer from optically oriented alkali metal atoms is being demonstrated in Cs – He, Rb – He, and K – He gas discharge plasmas; magnetometric devices using this effect have been created [130–132]. A test of an alkali–helium magnetometer showed [133, 134] that a 20–50% modulation of pumping parameters caused readings to shift by less than 0.01 nT MSE. The systematic component of the error was below 0.15 nT across the entire EMF range and random error only 0.02 nT. This resolution was achieved for the integration times 1 s, these instruments being rather slow.

4.3.6 Potassium narrow-line magnetometer. Unlike cesium and other alkaline-earth metals, ground-state potassium has an almost fully resolved system of magnetic resonances in the geomagnetic field; it is therefore possible to isolate a single line and largely disregard other spectral lines (Fig. 11). The line vertex is virtually independent of the pumping conditions; anyway, the dependence is measured in pico-Teslas rather than nano-Teslas, as with the entire cesium line. This accounts for the attractiveness of using potassium in the precision measurement of magnetic fields. The first attempts to this effect for OPQMs dating to the 1960s [135] were unsuccessful due to the difficulty of working with a structure containing several resonance lines. The first M_z-type potassium narrow-line magnetometer was constructed by the Geofizika Research and Manufacturing Association [136] and its most promising M_x-modification at the S I Vavilov State Optical Research Institute [20, 21]. At present, this work is underway at the Ioffe Physical Technical Institute.

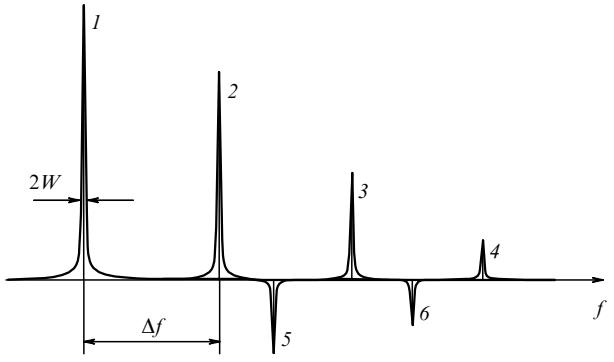

Figure 11. Magnetic resonance spectrum of potassium isotope ^{39}K, ^{41}K in the EMF ($B \approx 50$ μT, $f \approx 350$ kHz). $2W \approx 1$ Hz is the total resonance linewidth, Δf is the splitting of magnetic resonance lines (in EMF $\Delta f \approx 0.5$ kHz for ^{39}K and $\Delta f \approx 1$ kHz for ^{41}K). Spectral lines *1–4* are transitions within the Zeeman structure of the $F = 2$ level: *1*, $m_F = -2 \leftrightarrow m_F = -1$; *2*, $m_F = = -1 \leftrightarrow m_F = 0$; *3*, $m_F = 0 \leftrightarrow m_F = 1$; *4*, $m_F = 1 \leftrightarrow m_F = 1$; lines *5, 6* are transitions within the Zeeman structure of the $F = 1$ level: *5*, $m_F = -2 \leftrightarrow m_F = 0$; *6*, $m_F = 0 \leftrightarrow m_F = 1$.

In what follows, we consider factors determining the accuracy and sensitivity of potassium narrow-line magnetometers. Each individual resonance in the potassium Zeeman spectrum is to a greater or lesser extent subject to the effect of adjacent resonances. The degree of isolation of a distinguished resonance depends on the ratio of the width of one line to the distance separating it from the nearest line. When M_x-type signals are used, the influence of the neighboring resonance wing on the frequency of the distinguished resonance is described by the quantity $\Delta\omega \approx \alpha\Gamma(\Gamma/\Delta)$, where $\alpha < 1$ is the relative magnitude of adjacent resonance, Γ is its width, and Δ is the distance to the nearest line. This expression holds for $\Delta \gg \Gamma$. For M_z-signals, the influence of the neighbor resonance is much smaller [proportional to $\alpha\Gamma(\Gamma/\Delta)^3$].

The distance Δ for ^{39}K and ^{41}K in a mean EMF is of the order of 0.5 and 1 kHz, respectively. At a resonance width of 1 Hz, the frequency shift of the main resonance under the effect of the adjacent one is smaller than 1/500 Hz for ^{39}K, in agreement with the maximum error of field measurement (~ 0.3 pT), which is four orders of magnitude smaller than the systematic error of Cs magnetometers. Although errors of different origins may predominate in practical measurements, the limiting accuracy of isolated-line magnetometers is nevertheless much higher than that of Cs magnetometers using an unresolved line.

The use of a resonance line as wide as one or a few Hertz in an M_z-scheme would result in a rapid loss of operational speed (this can be avoided in the so-called *tandem* design discussed in Section 4.3.7 below). M_x-magnetometers are natural subjects for the use of isolated narrow lines because their operational speed is not limited by linewidth. However, creation of a self-generating M_x-type K-magnetometer encounters the difficulty of preventing the multifrequency generation on the totality of spectral lines of the magnetic resonance. Mosnier [135] was the first to undertake generation on a single isolated K-line and use it to measure a magnetic field (see [104] for a detailed description of the experiment). This attempt failed because the author sought single-frequency generation by decreasing the radiofield amplitude and eventually obtained a signal indistinguishable against the background noise.

Both the self-generating and non-self-generating variants of the potassium narrow-line magnetometer were realized in the laboratory of E B Aleksandrov [13–15, 20, 21]. Self-generation at the isolated line $|F = 2, m_F = 1\rangle \rightarrow |F = 2, m_F = 2\rangle$ was achieved by introducing automatic regulation of amplification in the feedback loop to ensure single-line generation. An interesting modification of the self-generating M_x-magnetometer was proposed in a later work [137] to resolve the problem of identification and isolation of the resonance line in a complex spectrum. This instrument operates simultaneously at two extreme frequencies of the Zeeman spectrum coupled by the frequency of the external generator admixed to their common self-generation spectrum; this admixed frequency is roughly equal to the difference between the extreme frequencies. The frequency of the generator should be adjusted within narrow bounds to the magnetic field. In this scheme, polarization optical pumping is replaced with the alignment of Zeeman sublevels of the $F = 2$ level by light polarized perpendicular to the direction of the magnetic field. Resonance is detected from a signal produced by the Faraday rotation of the pump light polarization plane. The resonance signal at the frequency

equal to half the sum of extreme resonance frequencies is linear up to small cubic correction and is not subject to a light shift because the pumping light equally displaces both resonance transitions.

Physically (under the condition of suppression of generation at adjacent lines), the operating principle of the 'standard' self-generating potassium M_x magnetometer is analogous to that of the Cs magnetometer described in Section 4.3.1. One specific feature of the K-magnetometer is worthy of special note however: the set of several resonance lines in the potassium spectrum limits the measurement rate at a scale of the distance between adjacent resonances, although the speed of response of the self-generating M_x-magnetometer is theoretically unlimited. The limitation thus imposed on the measurement rate can be interpreted as follows. Fast random frequency modulation of the resonance-exciting radiofield gives rise to harmonics in its spectrum coincident with the frequency of neighbor line contours in which they induce resonances with random phases and amplitudes. This effect can be avoided by artificially limiting the feedback band of the M_x magnetometer. Moreover, practical application of high-performance self-generating M_x magnetometers (both potassium and cesium ones) is hampered by the necessity to rapidly measure the frequency of a noisy signal. In principle, the accuracy of such a measurement, δF, depends on the measurement time τ and the signal/noise ratio in the $1/\tau$ band (see Section 4.2). Anyway, measurement of the magnetic resonance frequency signal to a relative accuracy of 10^{-8} for $10^{-2}-10^{-1}$ s is a difficult task even at a sufficiently high signal-to-noise ratio and requires the use of sophisticated technologies. Also, there is no trivial technical solution to the problem of formation of a 90° resonance phase shift signal in the amplification loop taking into account phase delays introduced by the photodetector and amplifier of the signal.

It the past, these considerations taken together gave an incentive to design and development a non-self-generating M_x magnetometer (PLL magnetometer).

We consider the mode of operation of such a device. First, we turn to expressions (17) describing the amplitudes of the two orthogonal components of magnetization in the rotating reference frame in the process of magnetic resonance. In the laboratory system of coordinates, they are matched by the two quadrature components at the rf field frequency, i.e., phase-shifted by 90°. It is always possible to separate the u component in the mixed output signal from the photodetector by the phase detection method with a proper reference voltage phase. The u signal is noticeable in that it passes through zero at the exact resonance and changes sign on either side of it; the value of the u signal in the vicinity of the resonance center is proportional to the frequency difference of the resonance and the applied rf field. It allow using such a signal to control the frequency of the reference resonance-inducing generator.

The basic component of this scheme is a voltage-controlled oscillator (VCO), controlled by the output voltage of the phase detector fed on the one hand with a signal from the photodetector (carrying information about the phase and the amplitude of the pumping light after it passed through the cell) and on the other hand with the voltage of the generator producing an alternating magnetic field. The initial phase of the reference voltage must be set in advance. Under these conditions, the frequency of the reference generator is locked to any resonance into the vicinity of which it is forcibly brought. This poses the problem of the preliminary choice of resonance.

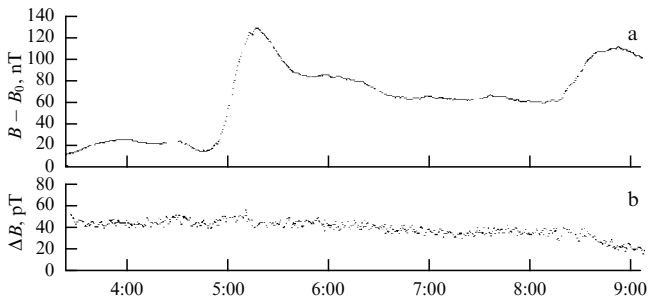

Figure 12. Variations in the magnetic field modulus (a) and its gradient (b) recorded by two K-magnetometers spaced 2 m apart at the SP-30 station (24 April 1989).

The advent of high-frequency digital frequency synthesizers (DFSs) provided a basis for the creation of digital PLL circuits not only for M_x-magnetometers but also for a potassium HFS magnetometer ($f = 460$ MHz). Microprocessors handle and analyze signals in real time, hence the possibility of designing schemes for tracking and measuring the magnetic resonance frequency in the complicated structure of resonance lines. In addition, such schemes permit simultaneously realizing sensitivity, accuracy, and operational speed determined by parameters of magnetic resonance over the entire range of geomagnetic fields [138, 139].

The metrological potential of K-magnetometers covers the full range of the Earth's magnetic fields with a record-breaking resolving power of the order of 100 fT $\text{Hz}^{-1/2}$ for standard lamp-pumped devices. As shown in the experiment in [15] and predicted in Refs [93, 95], laser pumping of a cell up to 15 cm in diameter allows increasing the resolving power to 1–3 fT $\text{Hz}^{-1/2}$. Systematic errors by the K-magnetometer are extremely small as a direct result of a narrow resonance and the minimal influence of adjacent lines, while its accuracy is much higher than the measurement accuracy of the magnetic field induction achieved thus far. Today, the absolute accuracy of K-magnetometers is estimated at 10–20 pT in the Earth's fields; this roughly corresponds to the accuracy with which fundamental constants necessary to convert the resonance frequency to the magnetic field induction have been estimated.

The attainable absolute accuracy is in a way characterized by the reproducibility of instrument readings from one switch-on to another and by their comparison over a long time with the readings of similar devices operated in a common uniform field. Figure 12 shows variations in field modulus for 6 hours and the difference between the readings of two K-magnetometers placed 2 m apart in an ice field close to the North Pole (SP-30 polar station, 1989). The difference did not exceed 40 pT. The frequency readings of both devices were simultaneously recorded at intervals of 1 s and a quantum digitization of 0.01 Hz, i.e., about 14 pT. This means that the 'legitimate' instrumental dispersion of the readings must be within 28 pT (assuming ideal stability of the magnetic field). The observed slight excess of the difference noise (especially its slow component) is easy to account for by the drift of the horizontal EMF gradient under the effect of nonstationary ionospheric sources of the magnetic field and by chaotic movements of the ice field in the nonuniform EMF [140]. It can be seen (Fig. 12a) that the

field modulus varied within 130 nT for 6 hours. In connection with this observation, we emphasize the difficulty of experimental verification of the sought long-term stability of magnetometer readings, which has a bearing on the problem of attainable field stability.

4.3.7 M_z-M_x tandem. To meet the contradictory requirements that a metrological instrument should have both high accuracy and high operational speed, two different devices are combined into a single system in which readings of the fast one are corrected by the other, which is slower but more accurate. This principle underlies modern timekeeping systems, in which the frequency of quartz or dielectric sapphire resonator is corrected by the error signal from the atomic frequency discriminator. A similar approach was proposed by Allen and Bender in 1972 [141] to accurately measure the modulus of the magnetic field induction. A magnetometer of this type consists of two OPQM modules, one designed as a spin generator (M_x-OPQM) whose output frequency automatically adjusts itself to induction of the external field and the other (M_z-OPQM) operates as a passive radiospectrometer locked via the feedback loop to the chosen magnetic resonance line. The M_z-OPQM uses a magnetic resonance spectrum with the resolved line structure and thereby ensures high accuracy of resonance frequency measurements. In contrast, the M_x-OPQM generates a group of unresolved lines in the vicinity of the center of gravity and produces large systematic errors.

Both parts of the first tandem magnetometer [141] were filled with ^{87}Rb vapor. The choice of ^{87}Rb was far from optimal because the magnetic resonance spectrum of this isotope contains a group of lines, the distance between which in EMS at a minimal number of perturbations was only severalfold greater than their width. This disadvantage was overcome after many years by a group of researchers headed by E Pulz [142], who proposed a tandem in which Cs was used in the M_x-scheme and K in the M_z-scheme. The spectrum of K magnetic resonance, unlike that of Rb, is known to be well resolved over the entire EMF range, which excludes interference between the adjacent lines.

The Cs–K-tandem described in Ref. [142] combines Cs–M_x and K–M_z magnetometers such that the signal from the slower but more accurate M_z-device being used for gradual correction of the feedback loop characteristics of the faster M_x-magnetometer. The system has the response time 1 ms, the resolving power 10 pT, and the absolute accuracy 0.1 nT.

4.3.8 M_z-M_x-tandem utilizing four-quantum resonance. The Cs–K-tandem described in Ref. [143] differs from its precursors in several parameters. First, it contains a single sensor with the Cs–K cell instead of two. Second, the four-quantum resonance $m_F=-2\leftrightarrow m_F=2$ of the K ground-state sublevel $F=2$ is used as the M_z-resonance. The peculiar properties of the highest ($n=4$) multiplicity resonance (for the $F=2$ level) were first employed in the new instrument; this resonance is practically unshifted by the alternating field (Fig. 13). Moreover, its frequency (unlike the frequencies of all others) shows a strong linear dependence on the induction of a constant magnetic field.

The unique properties of a four-quantum resonance were studied in Refs [144, 145]. It was shown that in type $\Delta F=0$, the $\Delta m_F=|n|$ spectrum of n-quantum transitions, the highest resonance ($n=2F$) has a frequency practically independent

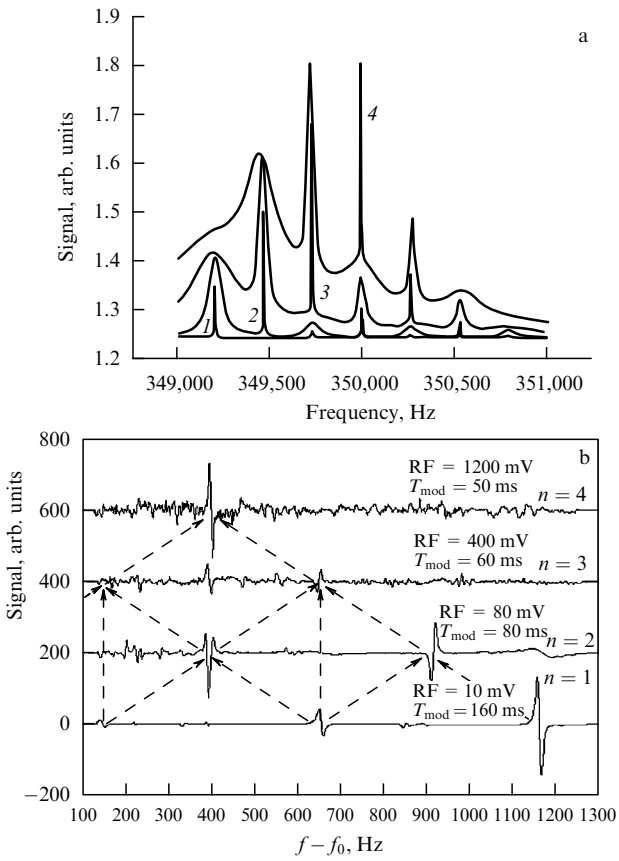

Figure 13. (a) Theoretical magnetic resonance spectrum in ^{39}K in the Earth's field for 4 values of the resonance radiofield amplitude. (b) Panoramic spectra of the signals of magnetic n-photon resonance ($n=1-4$) in the Zeeman structure of K obtained by low-frequency modulation of the resonant field frequency.

of the alternating field B_1. At its optimal strength, the four-quantum resonance has a width of several Hertz, whereas all other resonances are much wider; this removes the problem of seeking and maintaining the desired resonance.

The use of the four-quantum resonance in magnetometry encounters a difficulty arising from its narrowness that necessitates very slow scanning and accounts for a slowdown in the tracking system response. Therefore, the properties of four-quantum resonance were used based on a 'tandem' scheme combining a self-generating Cs magnetometer to ensure rapid reaction of the system as a whole with a four-quantum K-magnetometer providing a high absolute measurement accuracy and the linearity of the output frequency with respect to the field being measured.

The cesium spin oscillator scheme comprised a VCO locked to the frequency of the cesium resonance. Exact correction was performed using the signal of the four-quantum resonance in potassium by the introduction of an additional VCO frequency control loop.

Readings of the tandem remained stable within 10 pT under two-fold variations of the optical pumping intensity and changes of the working volume temperature by $\pm10\,^{\circ}$C; these values are certainly higher than variations that can be reasonably expected under real operational conditions.

4.3.9 Potassium narrow-line magnetometer with suppressed spin-exchange broadening. As mentioned above, the total angular momentum of the system is conserved in spin-

exchange processes, but coherence is destroyed; spin-exchange broadening increases with temperature in proportion to the concentration of atoms in the cell (28), rendering senseless all attempts to increase the sensitivity of a quantum magnetometer by increasing the temperature and, accordingly, the atom concentration. However, Happer and Tang showed in a 1973 experiment [66] that the spin-exchange broadening can be *decreased* by increasing the atomic concentration in weak magnetic fields, where the spin-exchange rate exceeds the Larmor frequency. Four years later, this effect was explained theoretically [67].

Since 2002, this has been the focus of interest of a Princeton group headed by M Romalis. The researchers proposed a variant of the highly sensitive magnetometer operating in superweak magnetic fields and characterized by suppressed spin-exchange broadening [146–149]. It was shown that under certain conditions, the influence of the spin-exchange broadening on the sensitivity of the magnetometer can be made negligibly small.

The density matrix of an alkali atom in the absence of rf fields coupling the hyperfine sublevels can be written as the sum of contributions from the hyperfine components a ($F = I + 1/2$) and b ($F = I - 1/2$): $\rho = \rho_a + \rho_b$. The total angular momentum of either state is expressed as

$$\mathbf{F}_a = \mathrm{Tr}\,[\mathbf{F}\rho_a]\,, \qquad \mathbf{F}_b = \mathrm{Tr}\,[\mathbf{F}\rho_b]\,. \tag{53}$$

In a magnetic field, both momenta precess with a speed ω_0 in opposite directions:

$$\begin{aligned} \frac{\mathrm{d}\mathbf{F}_a}{\mathrm{d}t} &= -\omega_0\,\mathbf{B}\times\mathbf{F}_a\,, \\ \frac{\mathrm{d}\mathbf{F}_b}{\mathrm{d}t} &= \omega_0\,\mathbf{B}\times\mathbf{F}_b\,. \end{aligned} \tag{54}$$

The total angular momentum of the system is conserved during spin-exchange collisions, while the degree of polarization in the two hyperfine states tends to be equated. We consider the precession of the total angular momenta initially parallel to the y axis around the field B_z. If the time between spin-exchange collisions T_{SE} is much smaller than the precession frequency period, the angle between $\mathbf{F}_a$ and $\mathbf{F}_b$ is also small, and it is possible to write the equation for the y-component of the momentum rotating with the total angular velocity ω:

$$-\omega_0\,\mathrm{d}t\,F_{ay} + \omega_0\,\mathrm{d}t\,F_{by} = \omega\,\mathrm{d}t\,(F_{ay} + F_{by})\,, \tag{55}$$

whence

$$\omega = \omega_0\,\frac{F_{ay} - F_{by}}{F_{ay} + F_{by}}\,. \tag{56}$$

In other words, the precession rate is expressed through the magnitude of polarization. As shown in Ref. [148], the transverse relaxation rate is

$$T_2^{-1} \approx \frac{1 - \cos\,(\omega_0 T_{\mathrm{SE}})}{T_{\mathrm{SE}}} \approx \omega_0^2 T_{\mathrm{SE}}\,. \tag{57}$$

This means that the transverse relaxation rate in weak fields decreases in proportion to H^2. This inference was confirmed experimentally. Indeed, the resonance width in weak magnetic fields (some 10 nT) in a K vapor cell at 170 °C (corresponding to $n \approx 3.7 \times 10^{13}$ cm^{-3}) did not exceed a few Hertz; conversely, it reached 350 Hz in a 300 nT magnetic field.

Under experimental conditions, the device worked as a many-channel gradient meter to exclude general field noises. ^{4}He was fed into the cell under a pressure of several atmospheres to slow down K diffusion and N_2 under 30 Torr to quench luminescence. The authors argue that the sensitivity obtained in a 0.3 cm^3 cell and magnetic fields below 0.2 mG was of the order of 1 fT Hz$^{-1/2}$ in the frequency range from 10 to 150 Hz. Complete nullification of two components of the magnetic field and reduction of the third one to a supersmall value (below 20 nT) were needed for the apparatus to function normally. This makes it unfit for application in geophysics. In a study with the use of a sensor in a system of magnetic coils nullifying the EMF [150], the sensitivity was three orders of magnitude lower (1 pT Hz$^{-1/2}$) than predicted; naturally, such a device is unable to measure magnetic fields in absolute terms because its accuracy is determined by magnetic coil parameters. Moreover, its Larmor frequency was related to the magnitude of polarization (see above). Nevertheless, this scheme perfectly illustrates a way to radically improve the metrological characteristics of a magnetometric device by decreasing the resonance linewidth.

4.3.10 Prototype magnetometer based on the electrically induced transparency effect. As mentioned in Section 3.4.6, broadening of the magnetic resonance line and, in the case of asymmetry, of the pump light spectral contour with respect to the line spectral contour, its shifts are directly proportional to the pumping intensity. Starting from certain intensity values characterized by the Rabi frequency $\Omega_{\mathrm{d}} \approx (\Gamma\Gamma_0)^{1/2}$ (where Γ is the optical transition width and Γ_0 is the magnetic transition width), light broadening becomes comparable with the intrinsic linewidth. Then, according to (37), the Q-factor of a quantum magnetometer ceases to increase with increasing pump light and thereafter begins to slowly decrease due to enhanced shot noises. The group of M Scully at the Max-Planck Institute, Germany, and at NIST, USA, developed a magnetometer free of this drawback [151–153].

A distinctive feature of this instrument is the use of a coherent three-level scheme (Λ-scheme) and measurement of the phase delay of the probe beam instead of a traditional absorption measurement. As shown in Ref. [151], the power broadening of the resonance line can be fully compensated by the phase measurement method in Λ-schemes with electromagnetically induced transparency (EIT). As usual, such schemes have three levels: two located close to each other (the ground level $|b\rangle$ and a metastable level $|c\rangle$ beneath) and the third $|a\rangle$ separated from them by an optical frequency. The levels $|a\rangle$ and $|c\rangle$ are coupled by a strong field whose Rabi frequency Ω_{d} is equal to the intrinsic width γ of the probe transition $|a\rangle \leftrightarrow |b\rangle$. The probe field has the Rabi frequency Ω_{p} ($\Omega_{\mathrm{p}} \ll \Omega_{\mathrm{d}} = \Gamma$). Both probe and strong fields are in a two-photon resonance, with the magnetic transition $|b\rangle \leftrightarrow |c\rangle$ having the intrinsic width Γ_0.

As in the traditional scheme, magnetic transition broadening begins at $\Omega_{\mathrm{d}} = (\Gamma\Gamma_0)^{1/2}$. However, a unique feature of the EIT transition is that the ratio of the probe transition dispersion to the absorption is determined by the inverse width of the magnetic transition Γ_0 and is independent of the strong field power if $\Omega_{\mathrm{d}} > (\Gamma\Gamma_0)^{1/2}$. Under conditions of a one-photon resonance ($\Delta = 0$) and a small two-photon

detuning δ,

$$\chi' \equiv \operatorname{Re}\chi \sim \frac{-\delta}{|\Omega_d|^2 + \Gamma\Gamma_0}\,, \qquad \chi'' \equiv \operatorname{Im}\chi \sim \frac{\Gamma_0}{|\Omega_d|^2 + \Gamma\Gamma_0}\,. \tag{58}$$

Thus, the reduced dispersion during an increase in the pumping strength can be compensated by an enhanced matter density at constant absorption. It is maintained that the Stark shift does not broaden the resonance but somewhat displaces it when the phase measurement method is used, in contrast to the traditional scheme where it leads to the effective resonance broadening under intense pumping (because it is proportional to the pumping intensity and varies in different cell regions). In a scheme that implies measurement of two circularly polarized components of probe light, the classical part of the Stark shift can be compensated.

At the same time, enhancement of the optical density and pumping intensity is associated with a new factor limiting the sensitivity of the magnetometer (quantum noises generated by the Stark shift nonuniform over the cell length). Calculations suggest that the maximum sensitivity is reached at $\Omega_d \sim (\Delta_0\Gamma_0)^{1/2}$ (Δ_0 is the effective detuning of the probe field). Unfortunately, information about the progress of this project is lacking in the literature, as are even rough estimates of the sensitivity and other characteristics of the instrument of interest. True, Ref. [153] reports the width of a 'narrow' resonance (3 kHz or more) obtained experimentally at the transition in an Rb hyperfine structure. Naturally, the achievement of a reasonably acceptable accuracy is out of the question at such linewidths that are hundreds of times those used in Cs magnetometers and thousand of times wider than in K magnetometers.

4.3.11 Prototype magnetometer based on the coherent population trapping effect. The coherent population trapping (CPT) effect is a sort of electrically induced transparency effect. The first report about a magnetometer based on a purely optical CPT effect was published by Wynands and co-workers (University of Bonn) in 1998 [154]. In that work, Cs atoms were simultaneously subjected to the light from two lasers tuned to 9.2 GHz or the HFS splitting frequency of ground-state cesium. The study was carried out in a 27 μT field with the fully resolved Zeeman structure of the HFS Cs spectrum. The authors used rapid modulation of the magnetic field to obtain a resonance line when scanning the relative detuning of the two lasers. The linewidth was roughly 10 kHz and the width of the asymmetric dip in the line center about 1 kHz. The signal-to-noise ratio was approximately 15 in the case of harmonic modulation of the external field with a 7 pT amplitude. Based on these values, the resolving power of the magnetometer was estimated at 500 fT.

Similar work is underway at NIST [155, 156], where a CPT magnetometer is being developed [157]. There are publications on this subject from the Lebedev Physical Institute, RAS, and the Institute of Laser Physics, Siberian Division of RAS [158]. NIST studies are carried out in the framework of an expensive project designed to develop a microminiaturized frequency reference [159, 160]. The Rb or Cs device will have a volume of the order of 1 cm^3 and a 10 mm^3 sensor.

Laser light is modulated at half the hyperfine transition frequency in the ground-state structure of working atoms. The laser carrier frequency is tuned such that lateral harmonics of the laser frequency ensure a two-photon resonance, coupling hyperfine sublevels of the ground state via the nearest excited state (the classical Λ-scheme). CPT resonances of the width 7 kHz are obtained in this scheme. Additional modulation of the laser light frequency is needed for locking to the center of the resonance line.

The same scheme can be operated (in principle) as a magnetometer by using a two-photon transition between two magnetodependent sublevels instead of magneto-independent ones. In other words, it is proposed to monitor the magnetic field in the cell of the highly miniaturized frequency standard. Certainly, the absolute accuracy of such a magnetometer is low according to the linewidth, and it is unsuitable for measuring the external magnetic field because the laser, the photodetector, and the heater located within 1 mm of each other produce rather high magnetic fields inside the cell. It is proposed in Ref. [156] to improve the parameters of the CPT magnetometer by the effect of nonlinear Faraday rotation, thoroughly investigated by D Budker and his group at the University of California, Berkeley.

However, the authors of Ref. [161] have recently dismissed the idea of using the CPT effect in a chip-scale magnetometer and returned to the standard detection of an M_x-resonance as ensuring higher accuracy and lower power consumption.

In 2001, the group of Wynands in Bonn studied the limiting characteristics of a magnetometer based on all-optical CPT effect. Paper [162] describes a scheme in which two lasers were substituted by one vertical-cavity surface-emitting laser (VCSEL) whose radiation was modulated with the frequency $\cong 4.6$ GHz. Although the 'dark' optical CPT resonance is not amenable to power broadening by laser light, it was nevertheless broadened due to the nonuniform Stark shift; this radically worsened the sensitivity of this magnetometric scheme.

The authors of Ref. [162] report on the 4 pT sensitivity of their magnetometer, estimated based on criterion (37) at measurement times starting from 1 s. They specify neither the accuracy nor shift values. Paper [163] describes the extension of this scheme, a gradient meter with pumping laser beams spaced 20 mm apart. Similarly to previous variants of the optical CPT magnetometer, this scheme is characterized by linewidths of the order of 1 kHz and a differential sensitivity of 26 pT. The authors consider the transition from the cesium D_2 line to the D_1 line as a way to improve the sensitivity because relatively fewer hyperfine components in the D_2-line spectrum are able to participate in the formation of a CPT resonance. Evidently, the choice of the D_2 line for pumping was dictated by the availability of a laser with $\lambda = 852$ nm.

We note that the first attempt to use the CPT effect in magnetometry was undertaken in Ref. [164], only CPT-inducing fields of the UHF range were used for the purpose rather than optical fields.

4.3.12 Magnetometer based on the nonlinear magneto-optical rotation effect. The nonlinear effect of magneto-optical rotation (nonlinear Faraday effect) is described as the dependence of the rotation angle of a quasi-resonant light polarization on both the magnetic field and light intensity, unlike in the linear Faraday effect characterized by the

absence of a light intensity dependence of the polarization rotation angle. The linear Faraday effect associated with the Zeeman splitting is attributable to the difference between refractive indices for two opposite circular components of linearly polarized light near the corresponding Zeeman transitions; the width of dispersion curves describing the linear effect is determined by the Doppler linewidth of the order of hundreds of megahertz. The nonlinear Faraday effect emerges at light intensities sufficiently high for the resonant modulation of medium properties. As a result, intense pumping may give rise to narrow resonances [165, 166], as in many other cases of laser nonlinear spectroscopy. The nonlinear Faraday effect is exemplified by an effect in the presence of the Lamb dip, i.e., a narrow dip in the atom distribution over velocities inside the cell during the interaction with monochromatic laser radiation. Budker and coworkers [167–170] proposed using the effect of polarization rotation arising from the resonant modulation of the pump light frequency. This effect is in essence very close to the well-known effect of paramagnetic resonance, induced when a harmonic system is affected by a frequency multiple of its resonance frequency, e.g., by the double resonance frequency.

The idea behind the method is as follows. Linearly polarized light tuned to resonance with an optical transition from the ground state and propagating parallel to the magnetic field aligns magnetic moments along the field. When the light frequency is modulated around the optical transition frequency with an amplitude wider than or comparable to the transition width at the frequency Ω_m, the resonance condition is satisfied twice during the modulation period; therefore, the medium properties change with the frequency $2\Omega_m$. The coincidence of this frequency with the Larmor frequency $\omega = \gamma B$ results in a parametric resonance, whose width is determined by the width of ground-state magnetic transitions. An additional advantage of this method is the possibility of directly observing polarization shifts at the Larmor frequency. The standard polarimetric schemes for the suppression of drifts and low-frequency fluctuations in an optical scheme use additional modulators of polarization.

Resonances as narrow as 1.3 Hz obtained in experiment are believed by the authors to ensure a sensitivity of the order of 10^{-11} G $Hz^{-1/2}$ (or 1 fT $Hz^{-1/2}$) in superweak magnetic fields ($\ll 100$ nT).

Paper [171] describes a magnetometer using the effect of nonlinear magneto-optical rotation in the Earth's field, where magnetic transitions are split due to the nonlinear Zeeman effect. The method used under these conditions allows, in principle (if a relatively powerful low-noise laser pump source is available), achieving a sensitivity of the order of 6×10^{-10} G $Hz^{-1/2}$ (or 60 fT $Hz^{-1/2}$).

4.3.13 Prototype magnetometer using 'quantum beats' with coherent excitation of Zeeman structure levels. Romalis at al. [172] (Princeton) described a way to significantly improve the characteristics of quantum magnetometric devices using atomic structures with a complex Zeeman spectrum. The method is based on the quantum beat effect associated with the excitation by modulated light that was first demonstrated as long ago as the middle of the last century [61, 62] (see above). The method consists of forcing coherence between Zeeman sublevels and permits (in the case of potassium) enhancing the spin polarization by a factor of 6 (a 3.9-fold increase was actually achieved in experiment) compared with the theoretically attainable one during 'classical' optical pumping; this enhancement is reached without additional broadening of the magnetic resonance line. Romalis and coworkers proposed and verified two approaches to the creation of such coherent superposition of Zeeman sublevels, one by modulating laser radiation and the other by modulating the alternating field in regular radiocoils. The first approach is an all-optical one and implies pumping the $F = 2$ level of the ground-state K atoms by a laser beam modulated both at the Larmor frequency (to ensure the magnetic resonance excitation proper) and (additionally) at the quadratic splitting frequency in K. In the spectral representation, this modulation corresponds to a comb of harmonics separated by the frequency intervals $2\nu_{rev} = 2bB^2$. As a result, a magnetic resonance is effectively and coherently excited at all Zeeman sublevels and the quantum beat signal produced with the period $2/\nu_{rev}$ is detected by the probe laser. Under these conditions, the magnetic resonance spectrum is a symmetric narrow resonance at the Larmor frequency of the $F = 2$ level (strictly proportional to the magnetic field) surrounded by harmonics spaced $n2\nu_{rev}$ $(n = 1, 2, \ldots)$ apart, with the amplitude of neighbor harmonics being close to the central resonance amplitude. The second approach is equivalent to the first one except that the pumping is accomplished by unmodulated laser radiation and the alternating magnetic field additionally modulated at the frequency of quadratic Zeeman splitting is used to excite the resonance and create a superposition of Zeeman sublevels (as in the classical OPQM scheme).

One more advantage of the described pumping method (in both variants) is that the symmetric structure of the central resonance prevents its displacement by nearby resonances (see Section 4.3.6); this property is preserved at any tilt of the pumping beam with respect to the magnetic field. An obvious drawback of the scheme is the necessity of locking to the central resonance, which has to be selected from a variety of resonances with practically identical amplitudes.

4.3.14 Prospective lines of development of quantum magnetometry with the use of quantum optical techniques and laser atom cooling. As mentioned in Section 4.1, application of optical pumping to the rapidly developing field of atomic laser cooling is of great potential interest for quantum magnetometry [173, 174]. Due to the virtually total absence of many magnetic moment relaxation mechanisms characteristic of 'warm' atoms, magnetometric schemes based on cold atoms may have very narrow lines; an example can be found in Ref. [175], where a storage time of 300 s at 0.3 mK was achieved for Li atoms in a dipole nonresonant optical trap.

Moreover, application of quantum optics methods to cold atom ensembles can in principle further increase the resolving power of radio-optical devices owing to 'compression' of the associated quantum noises [176]. Equally interesting from the cognitive point of view is the use of principally new quantum mechanical objects, e.g., Bose–Einstein condensates (BECs), to measure magnetic fields. The spin moment precession of the ^{87}Rb Bose–Einstein condensate is reported in Ref. [177]; optical pumping was accomplished by traditional techniques and resonance detection by a nondestructive method (nonresonant probe beam). This allowed a transverse magnetization relaxation time of 670 ms to be achieved using a BEC sample roughly equal to the atomic lifetime in the trap and demonstrated the sensitivity to magnetic field variations at

the level of 0.9 pT and the spatial resolution of 10 μm. As emphasized in [17], atomic laser cooling in such experiments invariably leads to an enhanced measurement sensitivity, but the role of specific quantum mechanical properties of BEC in this process remains unclear.

In any case, it is very difficult to achieve magnetic 'purity' of the space surrounding atoms in laser cooling schemes, even in pulsed ones, where all optical and magnetic fields are switched off after completion of an optical pumping cycle, the more so in dipole traps, where atoms are drawn into the nonresonant alternating electric field gradient. Therefore, practical implementation of such devices is a matter for the distant future.

4.3.15 Vector magnetometry with the use of quantum sensors. Quantum magnetometers are scalar or modular instruments having important advantages over all other tools for measuring magnetic fields; their readings are virtually independent of the magnetic field direction. Nevertheless, this property makes them applicable to the measurement of magnetic field vector components.

Although the frequency of a magnetic resonance is unrelated to the field direction, its amplitude shows a dependence on the direction of the pumping and probe beams (under real conditions, the two beams merge into one directed at approximately 45° with respect to the magnetic field vector). However, this dependence is in itself too weak to be used for practical purposes. Moreover, derivatives of the signal amplitude with respect to sensor tilt angles vanish at the optimum pumping angle.

A more promising possibility for the use of scalar sensors in vector magnetometry is related to the dependence of the probe beam modulation phase on the beam direction with respect to the magnetic field. A variant of such a measuring scheme is considered in Ref. [178]. It uses two beams, L1 parallel to the field being measured and L2 normal to L1. The first beam ensures optical pumping of alkali atoms and the second serves as the probe. As a result of the resonant radiofield action on the system, L2 undergoes strong modulation due to the interaction with the phased transverse component of the atomic moment; the modulation signal is used in the magnetometer's self-generating loop.

L1 is not subject to modulation if it is exactly parallel to the magnetic field. Deviation of the field from the beam direction by the angle Θ produces a modulation signal with the amplitude proportional to Θ and the phase depending on the direction of field deviation. The modulation signal can be expanded into two orthogonal components corresponding to two components of the magnetic field. These components are recognized by the respective synchronous detectors, whose signals are fed into additional coils, nullifying transverse field variations. Thus, this scheme measures the modulus of the magnetic field F and its two transverse components in its own system of coordinates. According to the authors of Ref. [178], the device is characterized by the variational sensitivity of measurement of transverse components of the order of 0.1 nT per s and drifts of the order of 2–3 nT per day.

Many schemes based on the methods of calibrated field perturbation use a scalar sensor integrated into a three-dimensional system of magnetic coils, creating a succession of artificial fields perpendicular to the field being measured; these methods are reviewed in [179].

An example of the successful implementation of such systems is reported in Ref. [180], published by a group of

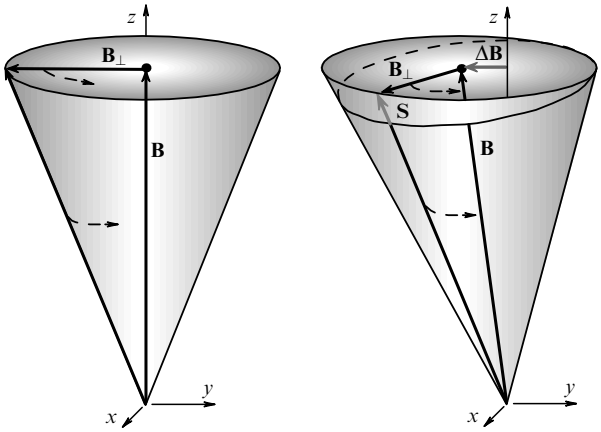

Figure 14. Vector diagram illustrating the work of a three-component variometer: **B** is the vector of the field being measured, **ΔB** is the field vector variation, $\mathbf{B}_\perp$ is the additional rotating field, and **S** is the signal.

French and Russian researchers in 2001. It describes an ^{4}He-vector magnetometer with laser optical pumping in which the helium sensor was placed in a system of magnetic coils, generating three roughly orthogonal alternating fields varying with three different frequencies (of the order of 10 Hz). The three field components were deduced from responses at the respective frequencies. The magnetometer had a sensitivity of 1 nT $\text{Hz}^{-1/2}$ and an operational of 1 Hz.

Precision measurement of variations of three magnetic field components is described in Ref. [181], along with the scheme of a vector magnetometer–variometer (VMV) based on this method. This apparatus is distinct from the devices described in the preceding paragraphs in that it uses (a) an optically pumped potassium sensor and (b) continuous fast rotation of the transverse magnetic field. The idea is to place a fast-operating magnetometer in the center of a highly stable coil system orientable in the EMF and creating an alternating magnetic field in the sensor, whose vector rotates conically around the EMF vector (Fig. 14). The coil system consists of two coils generating mutually orthogonal fields in the plane perpendicular to the EMF. The coils are excited by a sinusoidal current with a frequency f (tens or hundreds of hertz), the currents in the two coils being shifted in phase 90° relative to each other. These two orthogonal coils produce a field $B_\perp$, whose vector rotates with the frequency f in the plane normal to the EMF; the vector of the magnetic field created in the center of the system rotates conically with an angular opening about 5° with respect to the EMF vector.

Upon a change of transverse EMF components, the precession axis of the total magnetic field vector in the center of the system deviates from the EMF vector. This causes vector modulation at the frequency f (see Fig. 14). The signal at the modulation frequency f is used to induce fields *fully compensating* the respective transverse components of the EMF. The magnitude of currents in the coils generating these fields is regarded as a measure of the transverse components of the magnetic fields being measured.

One more variant of the VMV is described in Ref. [182]. This scheme differs from the previous one in that the introduction of 90–95% compensation of the EMF permits (1) increasing the sensitivity of measuring the transverse field components almost by an order of magnitude, (2) aligning the pumping axis and the axis of the magnetic field rotation cone, thereby eliminating potential systematic errors, and

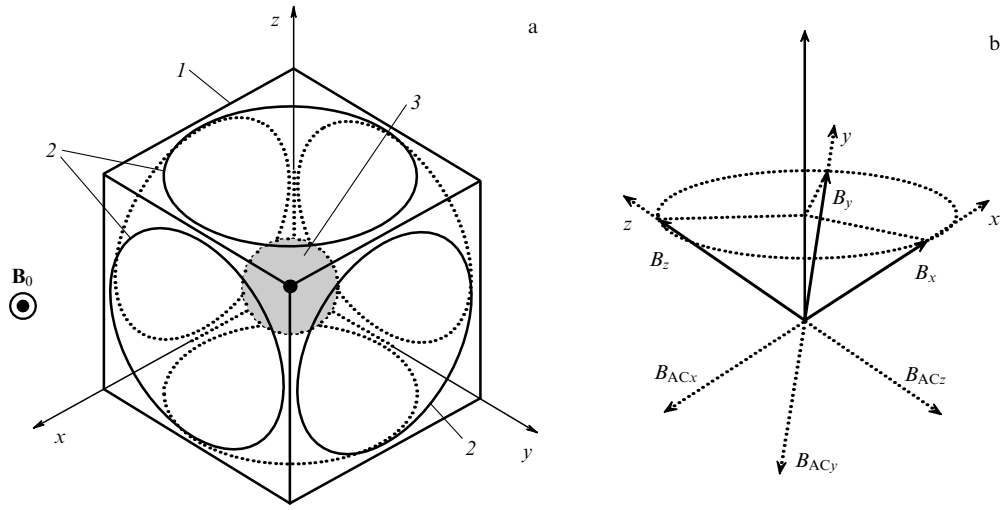

Figure 15. (a) Sensor in a three-component system of magnetic coils: *1* — cubic frame of the coil system, *2* — coils (current-carrying coils), *3* — sensor. The axis of the sensor and the vector of field $\mathbf{B}_0$ being measured are perpendicular to the drawing plane. (b) Projections B_x, B_y, B_z of the magnetic field $\mathbf{B}$ being measured and compensating the alternating field in coils B_{ACx}, B_{ACy}, B_{ACz} (maximum values). The axis of the sensor and the vector of field $\mathbf{B}_0$ being measured are parallel to the drawing plane. The circle in the *xyz* plane is a hodograph of the total magnetic field vector.

(3) using cesium as the working agent whose entire line in fields $B \leqslant 5$ μT has a sufficient degree of symmetry. The instrument based on this principle produced internal noises at the level of 0.010 – 0.015 nT r.m.s. at a 0.1 s sample rate, and the nonreproducibility of the *z*-channel not exceeding ±0.15 nT.

The method for the measurement of magnetic field components widely used in magnetic observatories consists of zeroing two field components and measuring a third one with the help of a scalar sensor [183]. It is easy to show that such a method does not require high nullification accuracy because, in accordance with the law of vector composition, the contribution of small transverse components to the field modulus in the presence of the large uncompensated component being measured is suppressed by a few orders of magnitude.

The principal disadvantage of this method is the impossibility of simultaneously or at least rapidly measuring all three components of the field at a single point. The way to simultaneously measure the three components of the EMF vector by an optical-pumping M_x-magnetometer integrated into a symmetric system of magnetic coils was proposed in [184]. This method provides high *absolute* accuracy and thereby differs from all other techniques for measuring field vector components with the help of the modular sensor described in the present section. The short-term sensitivity depends on the sensitivity of the M_x-magnetometer [15].

In this method, the sensor is surrounded by a system of compensating fields harmonically modulated such that the vector of the resultant magnetic field in the sensor rotates, retaining its length, around the initial field direction, and passes through three positions in each rotation cycle. In each position, two components of the magnetic field are compensated with high accuracy, while the third one is fully uncompensated and amenable to measurement (Fig. 15). It has been shown that the use of the M_x-magnetometer with optical pumping and the symmetric three-component system of magnetic coils as the sensor permits simultaneously measuring the three components of the EMF vector with an absolute accuracy of ±0.1 nT with a 0.1 s time response. Such a result is unattainable by any other known method.

5. Conclusion

To conclude, optical-pumping magnetometers may have numerous and diverse applications where the measurement of the magnetic field modulus and gradients, as well as field vector components, is needed. Problems requiring both high accuracy and high operation speed can be successfully solved by combining different types of quantum measuring devices. For all the variety of methods available to excite and detect magnetic resonance, the basic trend toward the improvement of field measuring systems is the narrowing of the magnetic resonance line; for the Earth's field range, this implies the use of atomic structures with well-resolved spectra, such as the HFS spectrum of alkali metals in the UHF region or the Zeeman spectrum of the potassium atom in the radio-frequency range.

References

1. Bloch F *Phys. Rev.* **70** 460 (1946)
2. Bloch F, Hansen W W, Packard M *Phys. Rev.* **70** 474 (1946)
3. Packard M, Varian R *Phys. Rev.* **93** 941 (1954)
4. Rabi I I *Phys. Rev.* **51** 652 (1937)
5. Rabi I I et al. *Phys. Rev.* **53** 318 (1938)
6. Overhauser A W *Phys. Rev.* **89** 689 (1953)
7. Overhauser A W *Phys. Rev.* **92** 411 (1953)
8. Carver T R, Slichter C P *Phys. Rev.* **92** 212 (1953)
9. Bitter F *Phys. Rev.* **76** 833 (1949)
10. Kastler A *J. Phys. Rad.* **11** 255 (1950)
11. Kastler A *J. Opt. Soc. Am.* **47** 460 (1957)
12. Aleksandrov E B *Optiko-Mekh. Promyshl.* **55** (12) 27 (1988) [*Sov. J. Opt. Technol.* (USA) **55** (12) 731 (1988)]
13. Alexandrov E B, Bonch-Bruevich V A *Opt. Eng.* **31** 711 (1992)
14. Alexandrov E B, Bonch-Bruevich V A, Yakobson N N *Opt. Zh.* **60** (11) 17 (1993) [*Sov. J. Opt. Technol.* **60** 756 (1993)]
15. Alexandrov E B et al. *Laser Phys.* **6** 244 (1996)
16. Alexandrov E B *Phys. Scripta* **T105** 27 (2003)
17. Budker D, Romalis M *Nature Phys.* **3** 227 (2007)
18. Jaklevic R C et al. *Phys. Rev. Lett.* **12** 159 (1964)
19. Carelli P et al. *Europhys. Lett.* **39** 569 (1997)
20. Aleksandrov E B et al. *Opt. Spektrosk.* **58** 953 (1985) [*Opt. Spectrosc.* **58** 439 (1985)]
21. Aleksandrov E B, Balabas M V, Bonch-Bruevich V A *Pis'ma Zh. Tekh. Fiz.* **13** 749 (1987) [*Sov. Tech. Phys. Lett.* **13** 312 (1987)]

22. de Zafra R L *Am. J. Phys.* **28** 646 (1960)
23. Benumof R *Am. J. Phys.* **33** 151 (1965)
24. Cohen-Tannoudji C, Kastler A, in *Progress in Optics* Vol. 5 (Ed. E Wolf) (Amsterdam: North-Holland, 1966)
25. Pomerantsev N M, Ryzhkov V M, Skrotskii G V *Fizicheskie Osnovy Kvantovoi Magnitometrii* (Physical Principles of Quantum Magnetometry) (Moscow: Nauka, 1972)
26. Kholodov Yu A, Kozlov A N, Gorbach A M *Magnitnye Polya Biologicheskikh Ob'ektov* (Magnetic Fields of Biological Objects) (M.: Nauka, 1987) [Translated into English (Moscow: Nauka Publ., 1990)]
27. Happer W *Rev. Mod. Phys.* **44** 169 (1972)
28. Brossel J, Kastler A *C.R. Acad. Sci., Paris* **229** 1213 (1949)
29. Brossel J, Bitter F *Phys. Rev.* **86** 308 (1952)
30. Franzen W, Emslie A G *Phys. Rev.* **108** 1453 (1957)
31. Dehmelt H G *Phys. Rev.* **103** 1125 (1956)
32. Manuel J, Cohen-Tannoudji C *C.R. Acad. Sci., Paris* **257** 413 (1963)
33. Bonch-Bruevich A M, Khodovoi V A *Usp. Fiz. Nauk* **93** 71 (1967) [*Sov. Phys. Usp.* **10** 637 (1968)]
34. Happer W, Mathur B S *Phys. Rev.* **163** 12 (1967)
35. Mathur B S, Tang H, Happer W *Phys. Rev.* **171** 11 (1968)
36. Bulos B R, Marshall A, Happer W *Phys. Rev. A* **4** 51 (1971)
37. Fano U *Rev. Mod. Phys.* **29** 74 (1957)
38. D'yakonov M I, Perel' V I *Zh. Eksp. Teor. Fiz.* **48** 345 (1965) [*Sov. Phys. JETP* **21** 227 (1965)]
39. Dehmelt H G *Phys. Rev.* **109** 381 (1958)
40. Bouchiat M A, Carver T R, Varnum C M *Phys. Rev. Lett.* **5** 373 (1960)
41. Walker T G, Happer W *Rev. Mod. Phys.* **69** 629 (1997)
42. Walters G K, Colegrove F D, Schearer L D *Phys. Rev. Lett.* **8** 439 (1962)
43. Schearer L D, Colegrove F D, Walters G K *Rev. Sci. Instrum.* **34** 1363 (1963)
44. Smirnov B M *Usp. Fiz. Nauk* **133** 569 (1981) [*Sov. Phys. Usp.* **24** 251 (1981)]
45. Keiser G M, Robinson H G, Johnson C E *Phys. Lett. A* **51** 5 (1975)
46. Blinov E V, Zhitnikov R A, Kuleshov P P *Pis'ma Zh. Tekh. Fiz.* **2** 305 (1976) [*Sov. Tech. Phys. Lett.* **2** 117 (1976)]
47. Blinov E V, Zhitnikov R A, Kuleshov P P, in *Geofizicheskaya Apparatura* (Geophysical Apparatuses) No. 76 (Leningrad: Nedra, 1982) p. 9
48. Schearer L D *Phys. Rev. Lett.* **22** 629 (1969)
49. Feynman R P, Vernon F L (Jr.), Hellwarth R W *J. Appl. Phys.* **28** 49 (1957)
50. Blum K *Density Matrix Theory and Applications* (New York: Plenum Press, 1981) [Translated into Russian (Moscow: Mir, 1983)]
51. Vanier J *Phys. Rev.* **168** 129 (1968)
52. Goppert-Mayer M *Ann. Physik* **9** 273 (1931)
53. Goppert-Mayer M *Naturwissenschaften* **17** 932 (1929)
54. Bonch-Bruevich A M, Khodovoi V A *Usp. Fiz. Nauk* **85** 3 (1965) [*Sov. Phys. Usp.* **8** 1 (1965)]
55. Hughes V, Grabner L *Phys. Rev.* **79** 314 (1950)
56. Hughes V, Grabner L *Phys. Rev.* **79** 819 (1950)
57. Kusch P *Phys. Rev.* **93** 1022 (1954)
58. Kusch P *Phys. Rev.* **101** 627 (1956)
59. Brossel J, Cagnac B, Kastler A *C.R. Acad. Sci., Paris* **237** 984 (1954)
60. Swain S *J. Phys. B* **15** 3405 (1982)
61. Bell W E, Bloom A L *Phys. Rev. Lett.* **6** 280 (1961)
62. Aleksandrov E B *Opt. Spektrosk.* **14** 436 (1963) [*Opt. Spectrosc.* **14** 232 (1963)]
63. Hahn E L *Phys. Rev.* **80** 580 (1950)
64. Das T P, Saha A K *Phys. Rev.* **93** 749 (1954)
65. Waller I *Z. Phys.* **79** 370 (1932)
66. Happer W, Tang H *Phys. Rev. Lett.* **31** 5 273 (1973)
67. Happer W, Tam A C *Phys. Rev. A* **16** 1877 (1977)
68. Bouchiat M A, Brossel J *C.R. Acad. Sci.* **254** 3828 (1962)
69. Bouchiat M A, Brossel J *Phys. Rev.* **147** 41 (1966)
70. Liberman V, Knize R J *Phys. Rev. A* **34** 5115 (1986)
71. Balabas M V, Bonch-Bruevich V A *Pis'ma Zh. Tekh. Fiz.* **19** (7) 6 (1993) [*Tech. Phys. Lett.* **19** 191 (1993)]
72. Balabas M V, Przhibel'sky S G *Chem. Phys. Rep.* **14** 882 (1995)
73. Balabas M V, Karuzin M I, Pazgalev A S *Pis'ma Zh. Eksp. Teor. Fiz.* **70** 198 (1999) [*JETP Lett.* **70** 196 (1999)]
74. Franzen W *Phys. Rev.* **115** 850 (1959)
75. McNeal R A *J. Chem. Phys.* **37** 2726 (1962)
76. Bernheim R A *J. Chem. Phys.* **36** 135 (1962)
77. Carver T R *J. Phys. Rad.* **19** 872 (1958)
78. Arditi M, Carver T R *Phys. Rev.* **136** A643 (1964)
79. Arditi M, Carver T R *Phys. Rev.* **112** 449 (1958)
80. Yi C S, in *Optical Pumping and Atomic Line Shape* (Warszawa: Państwowe Wydawn. Naukowe, 1969) p. 403
81. Czuchaj E, Fiutak J, in *Optical Pumping and Atomic Line Shape* (Warszawa: Państwowe Wydawn. Naukowe, 1969) p. 527
82. Brossel J *Ann. Physique* **7** 622 (1962)
83. Cohen-Tannoudji C *Ann. Physique* **7** 423 (1962)
84. Allan D W *Proc. IEEE* **54** 221 (1966)
85. Cohen-Tannoudji C et al. *Phys. Rev. Lett.* **22** 758 (1969)
86. Cramér H *Mathematical Methods of Statistics* (Princeton, NJ: Princeton Univ. Press, 1946) p. 477
87. Groeger S et al. *Eur. Phys. J. Appl. Phys.* **33** 221 (2006)
88. Mohr P J, Taylor B N *Rev. Mod. Phys.* **77** 1 (2005)
89. Alexandrov E B et al. *Zh. Tekh. Fiz.* **74** (6) 118 (2004) [*Tech. Phys.* **49** 779 (2004)]
90. Dehmelt H G *Phys. Rev.* **105** 1487 (1957)
91. Dehmelt H G *Phys. Rev.* **105** 1924 (1957)
92. Bloom A L *Appl. Opt.* **1** 61 (1962)
93. Aleksandrov E B *Zh. Tekh. Fiz.* **60** (3) 162 (1990) [*Sov. Phys. Tech. Phys.* **35** 371 (1990)]
94. Gornyi M B, Matisov B G *Zh. Tekh. Fiz.* **53** (1) 44 (1983) [*Sov. Phys. Tech. Phys.* **28** 25 (1983)]
95. Vershovskii A K, Pazgalev A S *Zh. Tekh. Fiz.* **78** (5) 116 (2008) [*Tech. Phys.* **53** 646 (2008)]
96. Bell W E, Bloom A L *Phys. Rev.* **107** 1559 (1957)
97. Ando S *Jpn. J. Appl. Phys.* **4** 793 (1965)
98. Ruddock K et al., Patent USA, No. 3,252,081 (1966)
99. Arditi M, Patent USA, No. 3,281,663 (1966)
100. Franz F A *Rev. Sci. Instrum.* **34** 589 (1963)
101. Andrianov B A et al. *Izmer. Tekh.* (10) 85 (1976)
102. Kozlov A N, in *Geofizicheskaya Apparatura* (Geophysical Apparatuses) No. 24 (Leningrad: Nedra, 1965) p. 86
103. Hardwick C D *Geophysics* **49** 2024 (1984)
104. Yabuzaki T, Ogawa T *J. Appl. Phys.* **45** 1342 (1974)
105. Bison G, Wynands R, Weis A *Appl. Phys. B* **76** 325 (2003)
106. Hardwick C D *Geophysics* **49** 2004 (1984)
107. Groeger S et al. *Eur. Phys. J. D* **38** 239 (2006)
108. Aleksandrov E B, Mamyrin A B, Sokolov A P *Opt. Spektrosk.* **34** 1216 (1973)
109. Aleksandrov E B, Mamyrin A B, Yakobson N N, Inventor's certificate No. 438345; *Bull. Izobret.* (45) 230 (1976)
110. Aleksandrov E B, Mamyrin A B, Yakobson N N *Izmer. Tekh.* **20** (7) 73 (1977)
111. Aleksandrov E B, Mamyrin A B, Yakobson N N *Zh. Tekh. Fiz.* **51** 607 (1981) [*Sov. Phys. Tech. Phys.* **26** 363 (1981)]
112. Aleksandrov E B, Vershovskii A K, Pazgalev A S *Zh. Tekh. Fiz.* **76** (7) 103 (2006) [*Tech. Phys.* **51** 919 (2006)]
113. Alexandrov E B, Primdahl F *Meas. Sci. Technol.* **4** 737 (1993)
114. Richards M G et al. *J. Phys. B* **21** 665 (1988)
115. Chupp T E et al. *Phys. Rev. A* **38** 3998 (1988)
116. Chupp T E et al. *Phys. Rev. Lett.* **72** 2363 (1994)
117. Moreau O et al. *J. Physique III* **7** 99 (1997)
118. Aleksandrov E B et al. *Usp. Fiz. Nauk* **141** 551 (1983) [*Sov. Phys. Usp.* **26** 1015 (1983)]
119. Colegrove F D, Franken P A *Phys. Rev.* **119** 680 (1960)
120. Keyser A R, Rice J A, Schearer L D *J. Geophys. Res.* **66** 4163 (1961)
121. Chéron B et al. *Opt. Commun.* **115** 71 (1995)
122. Chéron B, Gilles H, Hamel J *Eur. Phys. J. Appl. Phys.* **13** 143 (2001)
123. Iakobson N N, Aleksandrov E B *Zh. Tekh. Fiz.* **48** 1914 (1978) [*Sov. Phys. Tech. Phys.* **23** 1089 (1978)]
124. Gilles H, Hamel J, Cheron B *Rev. Sci. Instrum.* **72** 2253 (2001)
125. McGregor D D *Rev. Sci. Instrum.* **58** 1067 (1987)
126. Dmitriev S P, Zhitnikov R A, Okunevich A I *Zh. Eksp. Teor. Fiz.* **70** 69 (1976) [*Sov. Phys. JETP* **43** 35 (1976)]
127. Blinov E V, Zhitnikov R A, Kuleshov P P *Pis'ma Zh. Tekh. Fiz.* **2** 305 (1976) [*Sov. Tech. Phys. Lett.* **2** 117 (1976)]
128. Blinov E V, Zhitnikov R A, Kuleshov P P *Zh. Tekh. Fiz.* **49** 588 (1979) [*Sov. Phys. Tech. Phys.* **24** 336 (1979)]

129. Blinov E V, Zhitnikov R A, Kuleshov P P, Inventor's certificate No. 578630; *Bull. Izobret.* (40) (1977)
130. Blinov E V et al. *Zh. Tekh. Fiz.* **54** 287 (1984) [*Sov. Phys. Tech. Phys.* **29** 168 (1984)]
131. Blinov E V et al. *Zh. Tekh. Fiz.* **54** 2315 (1984) [*Sov. Phys. Tech. Phys.* **29** 1362 (1984)]
132. Dmitriev S P, Denisov D E *Zh. Tekh. Fiz.* **67** (6) 131 (1997) [*Tech. Phys.* **42** 704 (1997)]
133. Blinov E V et al., in *Tez. Dokl. Vsesoyuzn. Seminara po Opticheskoi Orientatsii Atomov i Molekul* (All-Union Seminar on Optical Orientation of Atoms and Molecules, Abstacts) (Leningrad, 1987) p. 22
134. Blinov E V et al., in *Tez. Dokl. Vsesoyuzn. Seminara po Opticheskoi Orientatsii Atomov i Molekul* (All-Union Seminar on Optical Orientation of Atoms and Molecules, Abstacts) (Leningrad, 1987) p. 24
135. Mosnier J *Ann. Geophys.* **113** 22 (1966)
136. Vasyutochkin G S, in *Metody Razvedochnoi Geofiziki. Parashchelochnye Kvantovye Magnitometry i Ikh Primenenie* (Methods of Prospecting Geophysics. Para-Alkaline Quantum Magnetometers and Their Applications) (Leningrad: NPO 'Geofizika', 1976) p. 19
137. Balabas M V, Bonch-Bruevich V A, Provotorov S V *Pis'ma Zh. Tekh. Fiz.* **15** (8) 1 (1989) [*Sov. Tech. Phys. Lett.* **15** 287 (1989)]
138. Vershovskii A K, Pazgalev A S *Zh. Tekh. Fiz.* **76** (7) 108 (2006) [*Tech. Phys.* **51** 924 (2006)]
139. Vershovskii A K, Aleksandrov E B *Opt. Spektrosk.* **100** 17 (2006) [*Opt. Spectrosc.* **100** 12 (2006)]
140. Aleksandrov E B et al. *Geomagnetism Aeronomiya* **32** (5) 158 (1992)
141. Allen J H, Bender P L *J. Geomagn. Geoelectr.* **24** 105 (1972)
142. Pulz E, Jäckel K-H, Linthe H-J *Meas. Sci. Technol.* **10** 1025 (1999)
143. Aleksandrov E B et al. *Zh. Tekh. Fiz.* **70** (7) 118 (2000) [*Tech. Phys.* **45** 931 (2000)]
144. Aleksandrov E B, Pazgalev A S *Opt. Spektrosk.* **80** 534 (1996) [*Opt. Spectrosc.* **80** 473 (1996)]
145. Alexandrov E B, Pazgalev A S, Rasson J L *Opt. Spektrosk.* **82** 14 (1997) [*Opt. Spectrosc.* **82** 10 (1997)]
146. Allred J C et al. *Phys. Rev. Lett.* **89** 130801 (2002)
147. Kominis I K et al. *Nature* **422** 596 (2003)
148. Savukov I M, Romalis M V *Phys. Rev. A* **71** 23405 (2005)
149. Savukov I M et al. *Phys. Rev. Lett.* **95** 63004 (2005)
150. Seltzer S J, Romalis M V *Appl. Phys. Lett.* **85** 4804 (2004)
151. Lukin M D et al. *Phys. Rev. Lett.* **79** 2959 (1997)
152. Zibrov A S et al. *Phys. Rev. Lett.* **75** 1499 (1995)
153. Zibrov A S et al. *Phys. Rev. Lett.* **76** 3935 (1996)
154. Nagel A et al. *Europhys. Lett.* **44** 31 (1998)
155. Kitching J et al. *IEEE Trans. Instrum. Meas.* **49** 1313 (2000)
156. Schwindt P D D, Hollberg L, Kitching J *Rev. Sci. Instrum.* **76** 126103 (2005)
157. Arimondo E, in *Progress in Optics* Vol. 35 (Ed. E Wolf) (Amsterdam: Elsevier, 1996) p. 257
158. Taichenachev A V et al. *Pis'ma Zh. Eksp. Teor. Fiz.* **80** 265 (2004) [*JETP Lett.* **80** 236 (2004)]
159. Schwindt P D D et al. *Appl. Phys. Lett.* **85** 6409 (2004)
160. Liew L-A et al. *Appl. Phys. Lett.* **84** 2694 (2004)
161. Schwindt P D D et al. *Appl. Phys. Lett.* **90** 81102 (2007)
162. Stähler M et al. *Europhys. Lett.* **54** 323 (2001)
163. Affolderbach C et al. *Appl. Phys. B* **75** 605 (2002)
164. Vershovskii A K, Pazgalev A S, Aleksandrov E B *Zh. Tekh. Fiz.* **70** (1) 88 (2000) [*Tech. Phys.* **45** 88 (2000)]
165. Kozlov M G *Opt. Spektrosk.* **67** 1342 (1989) [*Opt. Spectrosc.* **67** 789 (1989)]
166. Smirnov V S, Tumaikin A M, Yudin V I *Zh. Eksp. Teor. Fiz.* **96** 1613 (1989) [*Sov. Phys. JETP* **69** 913 (1989)]
167. Budker D, Yashchuk V, Zolotorev M *Phys. Rev. Lett.* **81** 5788 (1998)
168. Budker D et al. *Phys. Rev. A* **62** 043403 (2000)
169. Budker D et al. *Phys. Rev. A* **65** 55403 (2002)
170. Pustelny S et al. *Phys. Rev. A* **73** 23817 (2006)
171. Acosta V et al. *Phys. Rev. A* **73** 53404 (2006)
172. Seltzer S J, Meares P J, Romalis M V, physics/0611014
173. Wieman C E, Pritchard D E, Wineland D J *Rev. Mod. Phys.* **71** S253 (1999)
174. Phillips W D *Rev. Mod. Phys.* **70** 721 (1998)
175. O'Hara K M et al. *Phys. Rev. Lett.* **82** 4204 (1999)
176. Oblak D et al. *Phys. Rev. A* **71** 43807 (2005)
177. Higbie J M et al. *Phys. Rev. Lett.* **95** 50401 (2005)
178. Fairweather A J, Usher M J *J. Phys. E* **5** 986 (1972)
179. Lamden R J *J. Phys. E* **2** 125 (1969)
180. Gravrand O et al. *Earth Planets Space* **53** 949 (2001)
181. Alexandrov E B et al. *Meas. Sci. Technol.* **15** 918 (2004)
182. Vershovskii A K et al. *Zh. Tekh. Fiz.* **76** (1) 115 (2006) [*Tech. Phys.* **51** 112 (2006)]
183. Brown J et al., Geomagnetism Unit Report No. 1 (Sussex: Institute of Geological Sciences, 1969)
184. Vershovskii A K *Opt. Spektrosk.* **101** 324 (2006) [*Opt. Spectrosc.* **101** 309 (2006)]